

UNIVERSITÀ DEGLI STUDI DI MILANO

Facoltà di Scienze e Tecnologie

Laurea Triennale in Fisica

Lattice dynamics and geometric anharmonicity

Advisor:

Prof. Nicola Manini

Candidate:

Francesco Gnan

Matricola n° 945635

Lattice dynamics and geometric anharmonicity

Francesco Gnan
Dipartimento di Fisica, Università degli Studi di Milano,
Via Celoria 16, 20133 Milano, Italia

16th February, 2023

Abstract

We compare the effects of geometric anharmonicity on bidimensional crystals characterized by perfectly harmonic springs: the square and the hexagonal lattice. In particular, we evaluate the difference between the total potential energy of the system and the second- and third-order of its Taylor expansion in atomic displacements. The anharmonic terms are nonzero, despite the harmonicity of the atomic interactions, simply due to the lattice geometry. To evaluate the geometric anharmonicity quantitatively in realistic vibration conditions, we simulate the two crystals with a molecular-dynamics code. We excite single phonons at points of high symmetry at the edge of the first Brillouin zone, and we observe that, due to symmetry, the third-order term vanishes: the fourth-order term dominates anharmonicity. When we excite a random combination of phonons, instead, the third-order term becomes the leading one.

Advisor: Prof. Nicola Manini

Contents

| 1 | Intr | oductio | n | 3 | | |
|----|-------|-----------------------|----------------------------------------|----|--|--|
| 2 | The | Harmo | onic Approximation | 4 | | |
| | 2.1 | One D | vimensional Chain | 6 | | |
| | 2.2 | Two-D | Dimensional Crystal, Square Lattice | 7 | | |
| | 2.3 | Two-D | Dimensional Crystal, Hexagonal lattice | 11 | | |
| 3 | Thi | rd-Orde | er Taylor Expansions | 14 | | |
| 4 | Exp | ansion | Verification | 15 | | |
| | 4.1 | Secon | d-Order Terms | 16 | | |
| | 4.2 | Third- | Order Terms | 16 | | |
| | 4.3 | Highe | r-Order Terms | 17 | | |
| 5 | Nun | nerical | Simulations | 17 | | |
| | 5.1 | Square | e Lattice | 19 | | |
| | | 5.1.1 | Point-X Zone-Edge Phonon | 19 | | |
| | | 5.1.2 | Point-M Zone-Edge Phonon | 22 | | |
| | | 5.1.3 | Combination Of Phonons | 24 | | |
| | 5.2 | 5.2 Hexagonal Lattice | | | | |
| | | 5.2.1 | Point-K Zone-Edge Phonon | 25 | | |
| | | 5.2.2 | Point-M' Zone-Edge Phonon | 28 | | |
| | | 5.2.3 | Combination Of Phonons | 30 | | |
| 6 | Con | clusion | s | 30 | | |
| A | Dyn | amical | Matrix Method | 32 | | |
| В | Tayl | lor Exp | ansions | 33 | | |
| C | Erro | or Estin | nation | 35 | | |
| Re | feren | res | | 37 | | |

1 Introduction

Harmonic springs produce harmonic crystals only when connecting atoms in one dimensional chains. In higher dimensions, however, they interestingly generate anharmonic crystals. This phenomenon is known as "geometric anharmonicity" [1, 2].

We study examples of crystal lattices consisting of atoms interacting via a harmonic pairwise potential of the form:

$$V_{\text{tot}} = \frac{1}{2} \sum_{i=1}^{N} \sum_{j} \frac{K_{ij}}{2} \left(r_{ij} - r_{ij}^{\text{eq}} \right)^{2}.$$
 (1)

Here N is the number of atoms, the index j runs on the first and second nearest neighbors to the i-th atom and K_{ij} represent the force constant that quantifies the strength of the interaction; r_{ij} is the instantaneous distance between atoms i and j and r_{ij}^{eq} is their distance when all atoms sit at the equilibrium perfect-lattice configuration:

$$r_{ij} = \|\vec{r}_i - \vec{r}_j\| = \sqrt{\sum_{\xi} (\xi_i - \xi_j)^2}$$
, (2)

$$r_{ij}^{\text{eq}} = \|\vec{r}_i^{\text{eq}} - \vec{r}_j^{\text{eq}}\| = \sqrt{\sum_{\xi \in q} (\xi_i^{eq} - \xi_j^{\text{eq}})^2} , \qquad (3)$$

where $\xi = x, y, z$ and $\xi^{eq} = x^{eq}, y^{eq}, z^{eq}$.

In the Born-Oppenheimer adiabatic scheme [3], we study the dynamics of nuclei independently of electronic motion, which is supposed to contribute to generate the interatomic potential V_{tot} .

It is evident [3,4,5] that the total potential energy of a linear chain of atoms, forced to move in one dimension with harmonic pairwise interactions, coincides exactly with its own second-order Taylor expansion, as long as no atomic displacements exceed one lattice constant $a = |x_i^{eq} - x_{i\pm 1}^{eq}|$. Indeed, in one dimension $r_{ij} = x_{ij} = |x_i - x_{i+1}|$ and the potential in Eq.(1) becomes:

$$V_{\text{tot}} = \frac{K}{2} \sum_{i=1}^{N} (|x_i - x_{i+1}| - a)^2 = \frac{K}{2} \sum_{i=1}^{N} (x_{i+1} - x_i - a)^2 , \qquad (4)$$

as long as $|x_{i+1} - x_i| > 0$. Eq.(4) is a sum of polynomials of second degree: they have zero partial derivatives if the order of derivation exceeds the degree of the polynomial itself [6]. This is why the one-dimensional potential coincides with its second-order expansion and the resulting crystal is harmonic.

However, in higher dimensions this argument no longer holds. For example, J. Miglio [2] carried out a preliminary investigation on how the nonpolynomial function for the distance r_{ij} (2) affects the Taylor expansion in two dimensions, introducing terms of order greater than the second. In particular, he quantified the effects of geometric anharmonicity for a two-dimensional square crystal by calculating the difference between the exact potential energy of the system, obtained numerically through a molecular dynamics (MD) code, and its analytical second-order Taylor expansion.

The purpose of this thesis is to extend this research, by obtaining an explicit expression for the third-order expansion and comparing it to the exact potential. In addition, we conduct the same study in parallel for a lattice with hexagonal geometry.

This thesis is organized as follows: In Section 2, we recall the theory and known results for the harmonic lattice dynamics. In particular, we derive the second-order terms of the Taylor expansion of V_{tot} and we discuss the phonon dispersion curves for both geometries. Next, we report the third-order terms and a sketch of their derivation in Section 3. In Section 4 we verify the correctness of the analytical Taylor expressions previously obtained, by comparing them with the exact total potential energy, for small deviations away from the equilibrium geometry. Finally, in Section 5 we excite specific normal modes of oscillation of the two types of crystal and also combinations of several of them in molecular dynamics (MD) simulations, to investigate the effects of geometric anharmonicity in different contests.

2 The Harmonic Approximation

In this section we recall the main results of the harmonic theory of phonons. The phonon dispersion laws are obtained from the second order Taylor expansion of V_{tot} .

It is convenient to express all physical quantities as combinations of the main model constants, namely a, m and K, as listed in Table 1.

To obtain the harmonic approximation, we expand V_{tot} up to the second order in the displacements from the equilibrium position $u_{\xi_i} = \xi_i - \xi_i^{\text{eq}}$:

$$V_{\text{tot}} = V_0 + V_2 + o(u^3) = V_0 + \frac{1}{2} \sum_{i\xi, j\chi} D_{\xi_i, \chi_j} u_{\xi_i} u_{\chi_j} + o(u^3) , \qquad (5)$$

where ξ , $\chi = x$, y, z; indexes i, j = 1, 2, ..., N label individual unit cells of the crystal, which, both for the square lattice and the hexagonal lattice, contain one atom each. Linear

| Physical quantity | Units |
|-------------------|---------------|
| length | a |
| mass | m |
| spring constant | K |
| wave vector | a^{-1} |
| force | Ka |
| energy | Ka^2 |
| time | $\sqrt{m/K}$ |
| frequency | $\sqrt{K/m}$ |
| velocity | $a\sqrt{K/m}$ |

Table 1: Natural model units for all physical quantities in this work, expressed as unique combinations of the three main parameters that characterise the model: a, m, K.

terms vanish because the expansion is carried out around the equilibrium geometry. The constant term V_0 is irrelevant to the study of lattice dynamics and vanishes for the specific potential in Eq.(1).

$$D_{\xi_{i},\chi_{j}} \equiv \left. \left(\frac{\partial^{2} V_{\text{tot}}}{\partial u_{\xi_{i}} \partial u_{\chi_{j}}} \right) \right|_{\text{eq}}$$
 (6)

is the dynamical matrix of the crystal in real space. Using this matrix we can set up the classical equations of motion for the dynamics of the nuclei:

$$m\ddot{u}_{\xi_i} = -\sum_{j\chi} D_{\xi_i,\chi_j} u_{\chi_j} \ . \tag{7}$$

Given the lattice traslation vectors \vec{R}_i and substituting in Eq.(7) a solution of the form

$$\vec{u}_i(t) = \vec{A}(\vec{q}, \omega) e^{i(\vec{q} \cdot \vec{R}_i - \omega t)} , \qquad (8)$$

we obtain

$$-m\omega^2 A_{\xi} = -\sum_{i\chi} D_{\xi_i,\chi_j} e^{-i\vec{q}\cdot\left(\vec{R}_i - \vec{R}_j\right)} A_{\chi} .$$

Defining the dynamical matrix of the crystal in reciprocal space as

$$D_{\xi,\chi}(\vec{q}) \equiv \sum_{i} D_{\xi_{i},\chi_{j}} e^{-i\vec{q}\cdot\left(\vec{R}_{i}-\vec{R}_{j}\right)}, \qquad (9)$$

we can solve the following eigenvalue equation, in order to get the normal phonon modes of the crystal we are studying:

$$\left\| D_{\xi,\chi}(\vec{q}) - m\omega^2 \delta_{\xi\chi} \right\| = 0 . \tag{10}$$

The secular equation (10) produces d eigenvalues for each \vec{q} , where d is equal to the problem dimensionality. So, as \vec{q} varies within the first Brillouin zone (1stBZ), d phononic branches are formed, whose frequencies are described by the functions $\omega(\vec{q}, d)$.

Appendix A provides more detail on this standard method for calculating phonon dispersion frequencies for the d=2 dimensional case.



Figure 1: A monoatomic linear chain describing longitudinal phonons, due to the atoms being obliged to oscillate along the chain direction, in one dimension only. Periodic boundary conditions such that the displacements $u_{N+1} = u_1$ are applied, to avoid an abrupt termination and preserve lattice symmetry.

2.1 One Dimensional Chain

In this subsection we analyze a linear chain of equal atoms, such as the one in Figure 1.

The derivation of the longitudinal oscillation frequency as a function of q is an elementary exercise [3,4,5]. The result is:

$$\omega(q) = 2\sqrt{\frac{K}{m}} \left| \sin(\frac{qa}{2}) \right| . \tag{11}$$

Figure 2 reports the dispersion relation (11) in an extended-zone scheme.

In the long wavelength limit $(qa \ll 1)$ it is possible to derive the expression for the sound velocity in the chain v_s :

$$\omega \approx \sqrt{\frac{K}{m}} a q = v_s q , \qquad v_s \equiv \sqrt{\frac{K}{m}} a .$$
 (12)

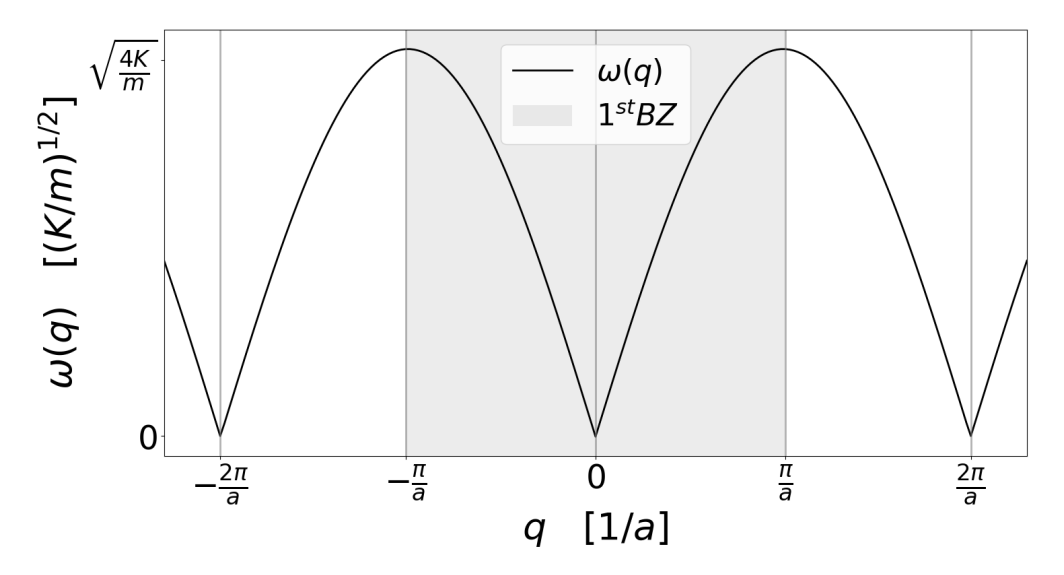


Figure 2: Oscillation frequencies of the linear chain as a function of the wavevector q. The curve is extended even outside the 1stBZ $\left[-\frac{\pi}{a}, \frac{\pi}{a}\right]$, greyed region, to highlight the translational symmetry in q space.

2.2 Two-Dimensional Crystal, Square Lattice

We start with the two-dimensional square lattice already investigated in Ref.[2]. Appendix B details how to calculate the Taylor expansion of the potential in Eq.(1). Unlike the one-dimensional chain, the two-dimensional crystal has two branches of acoustic phonons, which are labelled as the lower or transverse (T) acoustic branch and the upper or longitudinal (L) acoustic branch¹.

In the square lattice, at equilibrium, the nearest neighbors are distant a and the second neighbors are separated by a distance $a\sqrt{2}$. This is evident in Figure 3. For this reason, the interaction between the latter is expected to be weaker and characterized by a constant K' < K, where K is the force constant between nearest neighbors. Primitive vectors in the direct lattice are $\vec{a}_1 = a(1,0)$ and $\vec{a}_2 = a(0,1)$, while those of the reciprocal lattice are $\vec{b}_1 = \frac{2\pi}{a}(1,0)$ and $\vec{b}_2 = \frac{2\pi}{a}(0,1)$.

It is useful to fix a convention for the numbering of the first and the second neighbors of the i-th atom. We adopt the numbering in Figure 4a.

Figure 4b reports the first Brillouin zone, at the center of the reciprocal lattice. The 1stBZ is drawn in detail in Figure 5, where dots identify special symmetry points.

The second-order Taylor expansion of Eq.(1) was calculated by J. Miglio [2] and has the following form:

$$V_{2} = \frac{1}{2} \sum_{i=1}^{N} \left\{ 2 \left(K + K' \right) \left(u_{x_{i}}^{2} + u_{y_{i}}^{2} \right) - K \left[\sum_{j=1}^{2} u_{x_{j}} u_{x_{i}} + \sum_{j=3}^{4} u_{y_{j}} u_{y_{i}} \right] + \frac{K'}{2} \sum_{j=5}^{8} \left[(-1)^{j} \left(u_{x_{j}} u_{y_{i}} + u_{y_{j}} u_{x_{i}} \right) - \left(u_{x_{j}} u_{x_{i}} + u_{y_{j}} u_{y_{i}} \right) \right] \right\}.$$

$$(13)$$

Referring to the method outlined in Eqs.(5-10), the harmonic dispersion laws for normal modes of crystal vibration are:

$$\omega_{+/-} = \left\{ 2\frac{K}{m} \left[\sin^2 \frac{q_x a}{2} + \sin^2 \frac{q_y a}{2} + \frac{K'}{K} \left(1 - \cos q_x a \cos q_y a \right) \right] + \\ \pm 2\frac{K}{m} \left[\left(\sin^2 \frac{q_x a}{2} - \sin^2 \frac{q_y a}{2} \right)^2 + \left(\frac{K'}{K} \sin q_x a \sin q_y a \right)^2 \right]^{\frac{1}{2}} \right\}^{\frac{1}{2}} .$$
 (14)

The two solutions represent the frequencies of the longitudinal and transverse vibration, respectively:

$$\omega_{+} = \omega_{\rm L} , \qquad \qquad \omega_{-} = \omega_{\rm T} .$$

They are depicted in Figure 6.

Since the two-dimensional plots of Figure 6 are not easily readable, it is convenient to represent the frequencies as \vec{q} varies along the symmetry directions in Figure 5, as it is done in Figure 7.

¹They are named after the fact that the eigenvectors of the dynamical matrix are approximately perpendicular and parallel to the phonon wavevector \vec{q} , respectively.

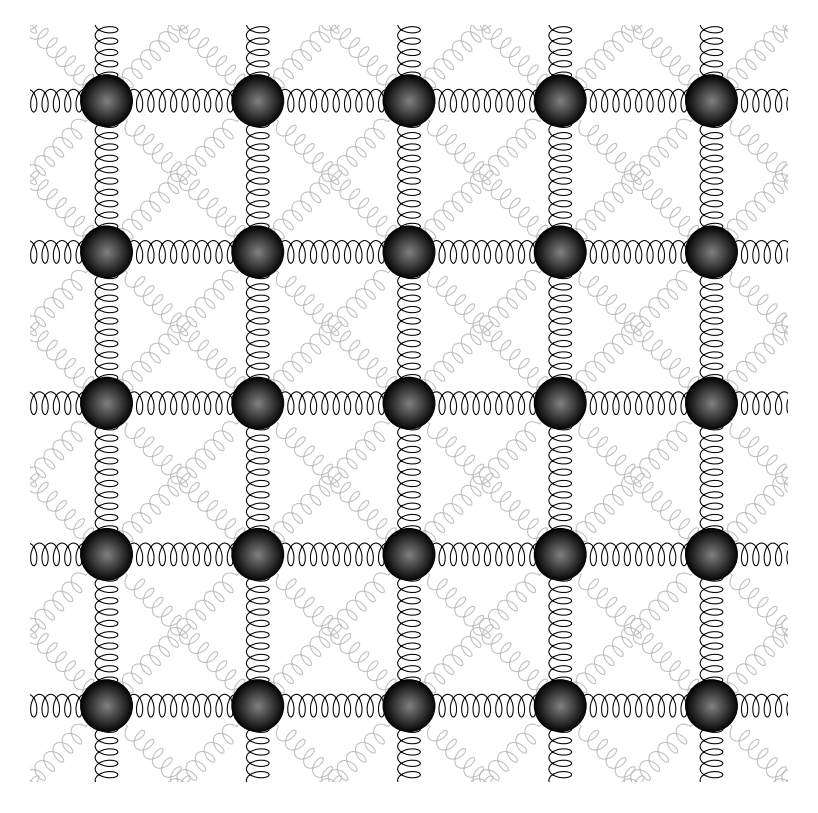


Figure 3: Square lattice with nearest (black springs) and next nearest (light gray springs) neighbors interactions. The lattice step is *a*. Periodic boundary conditions are supposed to be applied and then the crystal is regarded as infinite.

Considering Eq.(14) and calculating the limit for $|\vec{q}| \to 0$ and then dividing by $|\vec{q}|$, we derive the sound velocities in the two-dimensional square crystal. It is useful to represent \vec{q} in polar coordinates, $q_x = |\vec{q}| \cos \theta$ and $q_y = |\vec{q}| \sin \theta$.

$$v_{\rm L/T} = v_{+/-} = \sqrt{\frac{1}{2} + \frac{K'}{K} \pm \sqrt{\frac{1}{4}\cos^2(2\theta) + \left(\frac{K'}{K}\right)^2 \sin^2(2\theta)}} \quad a\left(\frac{K}{m}\right)^{\frac{1}{2}}$$
(15)

are nonzero for any K' > 0. In the special case K' = 0, the square-lattice instability is evident from the vanishing of certain sound velocities in specific \vec{q} directions, for example the transverse v_T for $\theta = 0$. If $K' = \frac{1}{2}K$, instead, we obtain two isotropic sound velocities:

$$v_{\rm L/T} = \sqrt{1 \pm \frac{1}{2}} \quad a \left(\frac{K}{m}\right)^{\frac{1}{2}} . \tag{16}$$

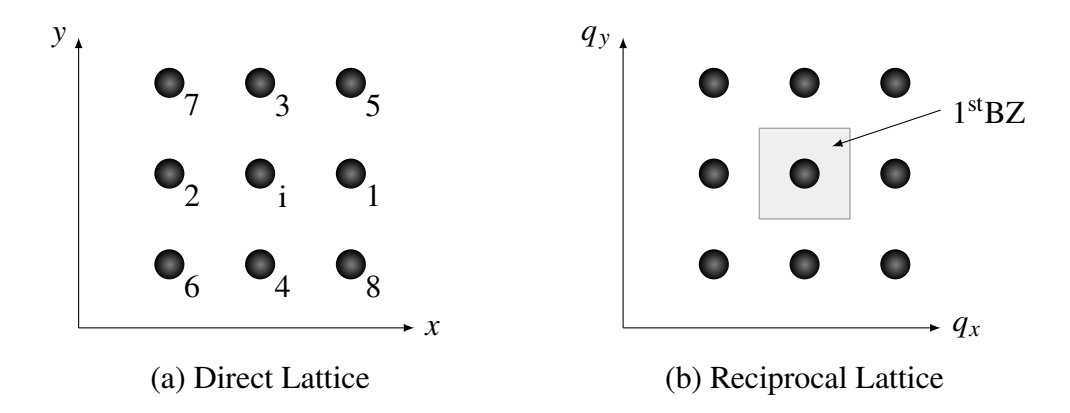


Figure 4: Panel a: the numbering convention for the j-th atom surrounding the i-th atom in the lattice. In panel b, instead, we show the reciprocal lattice and the 1stBZ.

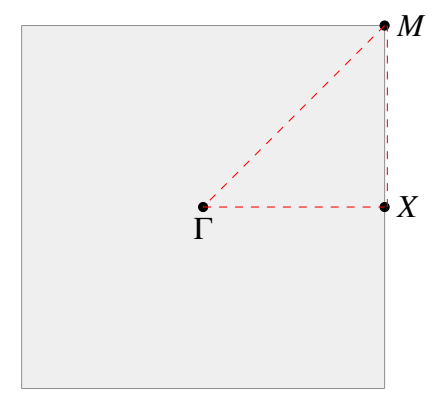


Figure 5: The 1stBZ of the square lattice. It has the shape of a square of side $\frac{2\pi}{a}$. The high-symmetry points have the following coordinates (q_x, q_y) in reciprocal space: $\Gamma = (0,0)$; $X = \frac{\pi}{a}(1,0)$; $M = \frac{\pi}{a}(1,1)$.

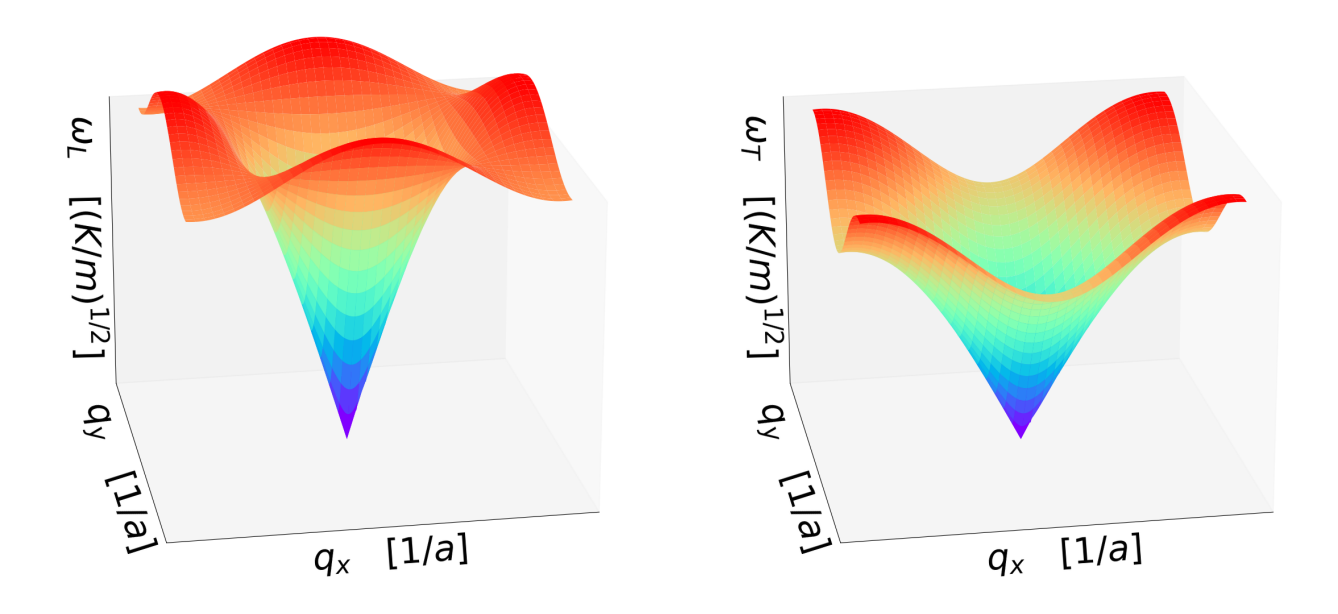


Figure 6: The two frequency dispersion laws of Eq.(14) as a function of \vec{q} inside the reciprocal square lattice with $q_x \in [-\frac{\pi}{a}, \frac{\pi}{a}]$ and $q_y \in [-\frac{\pi}{a}, \frac{\pi}{a}]$, namely the 1stBZ. ω_L is reported on the left, while ω_T on right.

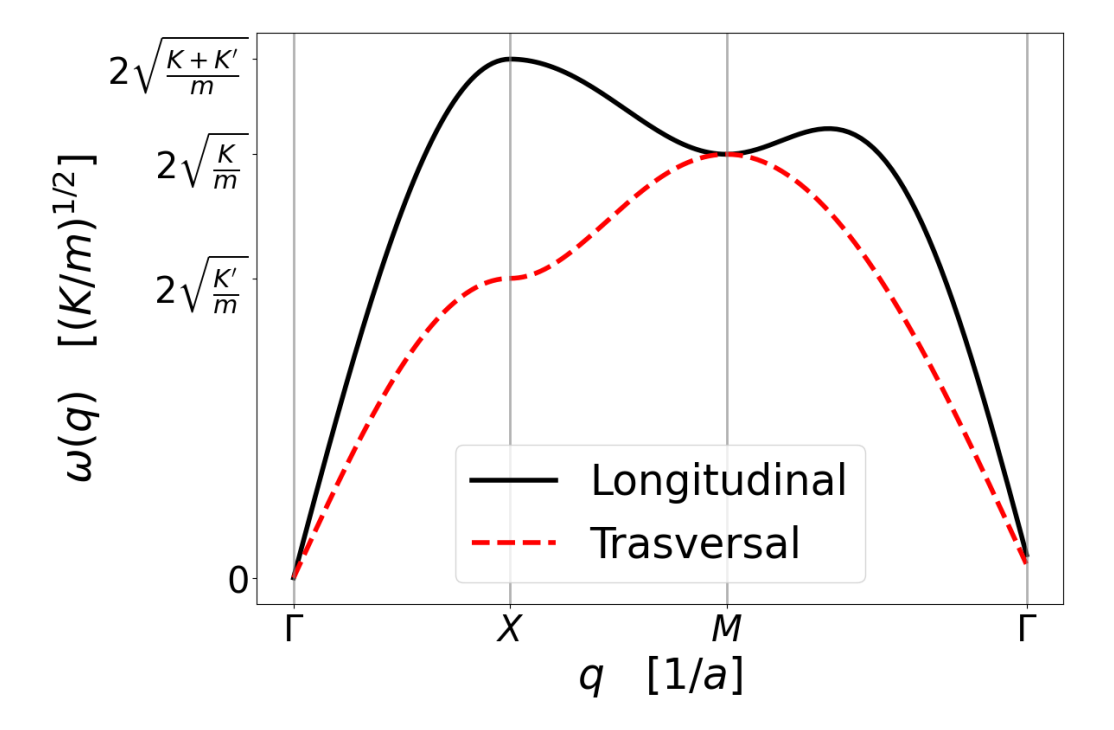


Figure 7: Phonon dispersion curve along the path $\Gamma - X - M - \Gamma$ inside the 1stBZ, as drawn in Figure 5. The fact that the slope of the dispersion curves is identical when arriving to Γ from different directions is an indication of the isotropy of the quadratic expansion terms for K' = 0.5K.

2.3 Two-Dimensional Crystal, Hexagonal lattice

Unlike the square geometry, in the hexagonal crystal the number of nearest and next nearest neighbors is 6 and their distances from the *i*-th atom are a and $\sqrt{3}a$, respectively. As before, the two types of interaction are characterized by K and K' < K. Figure 8 shows a region of a hexagonal lattice, where only the springs connecting the nearest neighbors are drawn. Figure 9a describes the numbering convention for neighbors adopted in this

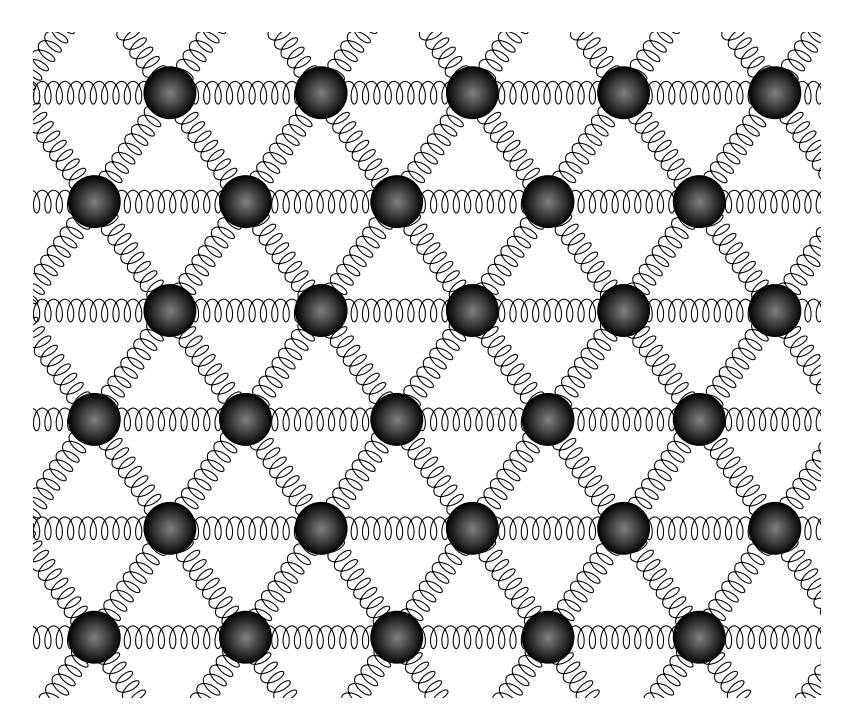


Figure 8: Hexagonal lattice with periodic boundary condition applied. In order to make the picture clearer, only the springs describing the interaction between nearest neighbors are depicted.

thesis. Figure 9b reports the reciprocal lattice with the 1stBZ. They are constructed as follows. First, we identify two primitive lattice vectors in direct space:

$$\vec{a}_1 = a(1,0)$$
, $\vec{a}_2 = a\left(-\frac{1}{2}, \frac{\sqrt{3}}{2}\right)$. (17)

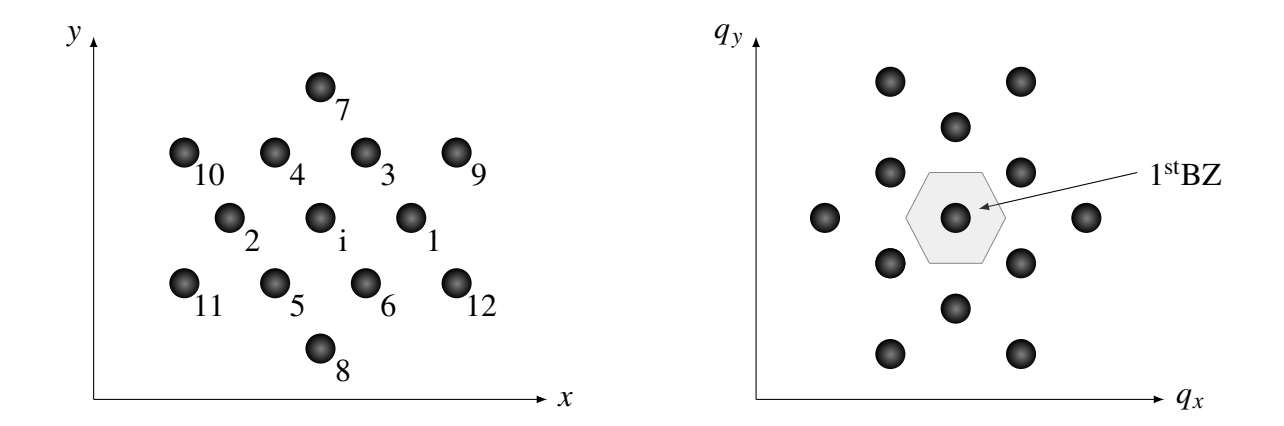
Then we calculate the corresponding ones in reciprocal space²

$$\vec{b}_1 = 2\pi \frac{\vec{a}_2 \times \hat{z}}{|\vec{a}_1 \times \vec{a}_2|} = \frac{2\pi}{a} \left(1, \frac{1}{\sqrt{3}} \right) , \qquad \vec{b}_2 = 2\pi \frac{\hat{z} \times \vec{a}_1}{|\vec{a}_1 \times \vec{a}_2|} = \frac{2\pi}{a} \left(0, \frac{2}{\sqrt{3}} \right) , \quad (18)$$

that generate the reciprocal lattice, Figure 9b. The 1stBZ can be obtained by drawing the bisector of the lines joining the nearest neighbors in the reciprocal lattice [3].

Referring to Appendix B, we calculate the second-order term of the Taylor expan-

²One can check the property $\vec{b}_i \cdot \vec{a}_j = 2\pi \delta_{ij}$.



(a) Direct Lattice

(b) Reciprocal Lattice

Figure 9: Direct (a) and reciprocal (b) hexagonal lattice. Atoms from 1 to 6 are nearest neighbors to the *i*-th; from 7 to 8 they are second neighbors.

sion of V_{tot} :

$$V_{2} = \frac{1}{2} \sum_{i=1}^{N} \left\{ 3 \left(K + K' \right) \left(u_{x_{i}}^{2} + u_{y_{i}}^{2} \right) - K \sum_{j=1}^{2} u_{x_{j}} u_{x_{i}} + \frac{K}{4} \left[\sum_{j=3}^{6} (-1)^{j} \sqrt{3} \left(u_{x_{j}} u_{y_{i}} + u_{y_{j}} u_{x_{i}} \right) - \left(u_{x_{j}} u_{x_{i}} + 3 u_{y_{j}} u_{y_{i}} \right) \right] +$$

$$- K' \sum_{j=7}^{8} u_{y_{j}} u_{y_{i}} + \frac{K'}{4} \left[\sum_{j=9}^{12} (-1)^{j} \sqrt{3} \left(u_{x_{j}} u_{y_{i}} + u_{y_{j}} u_{x_{i}} \right) - \left(3 u_{x_{j}} u_{x_{i}} + u_{y_{j}} u_{y_{i}} \right) \right] \right\}.$$

$$(19)$$

Following the method sketched in Appendix A, we derive the harmonic phonon oscillation frequencies. For simplicity, we take into account only the interaction between first neighbors (K' = 0).

$$\omega_{+/-} = \sqrt{\frac{K}{m}} \left\{ 3 - \cos(q_x a) - 2\cos\left(\frac{q_x a}{2}\right) \cos\left(\frac{\sqrt{3}q_y a}{2}\right) + \left[\cos^2(q_x a) + \cos^2\left(\frac{q_x a}{2}\right) \cos^2\left(\frac{\sqrt{3}q_y a}{2}\right) + \right.$$

$$\left. - 2\cos(q_x a) \cos\left(\frac{q_x a}{2}\right) \cos\left(\frac{\sqrt{3}q_y a}{2}\right) + 3\sin^2\left(\frac{q_x a}{2}\right) \sin^2\left(\frac{\sqrt{3}q_y a}{2}\right) \right]^{\frac{1}{2}} \right\}^{\frac{1}{2}} .$$

$$(20)$$

Using Eq.(20) one can once again graphically represent the longitudinal and transverse phonon dispersion curves, as in Figure 10.

Evaluating the limit for $|\vec{q}| \to 0$ yields two isotropic sound velocities, longitudinal and transverse:

$$v_{\rm L/T} = v_{+/-} = \frac{\sqrt{3}}{2} \sqrt{1 \pm \frac{1}{2}} \quad a \left(\frac{K}{m}\right)^{\frac{1}{2}}.$$
 (21)

The phonon dispersion curves are also reported along the high-symmetry directions in Figure 11. These symmetry paths can be seen in Figure 12.

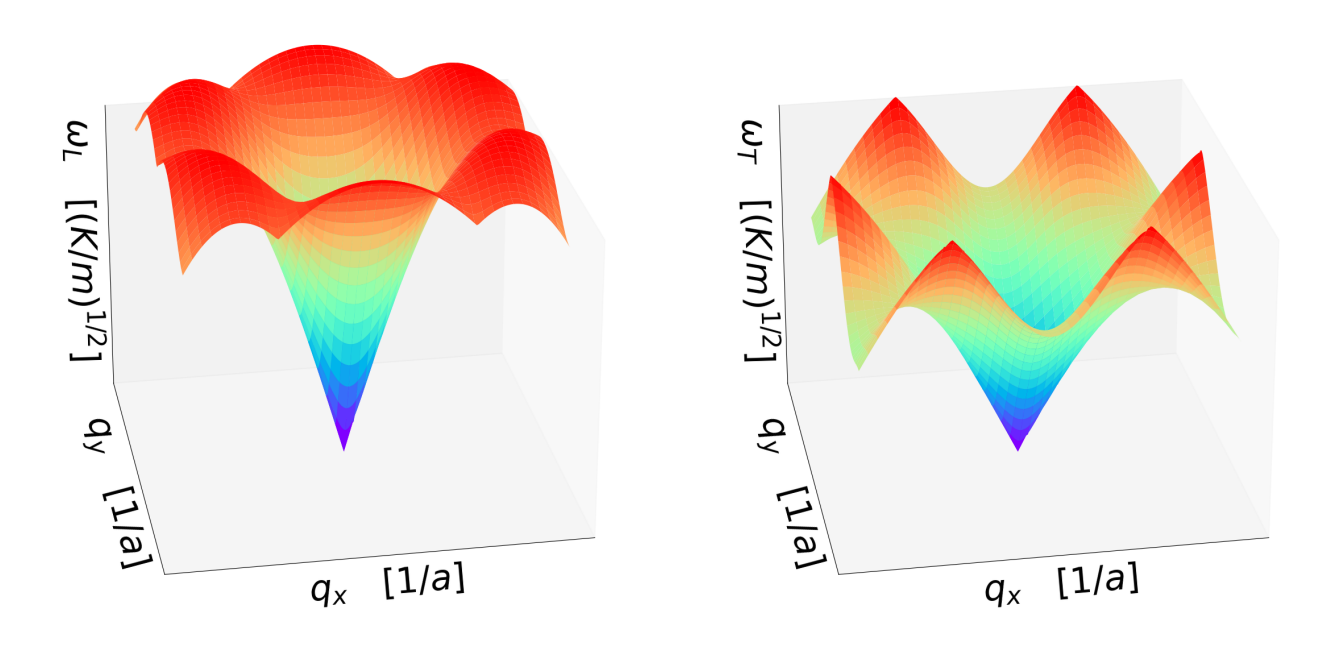


Figure 10: Phonon dispersion curves for the hexagonal lattice with nearest neighbors only (K'=0), Eq.(20), the \vec{q} vector spanning the rectangle $q_x \in [-\frac{4\pi}{3a}, \frac{4\pi}{3a}]$ and $q_y \in [-\frac{2\pi}{\sqrt{3}a}, \frac{2\pi}{\sqrt{3}a}]$, which covers the 1stBZ enterely.

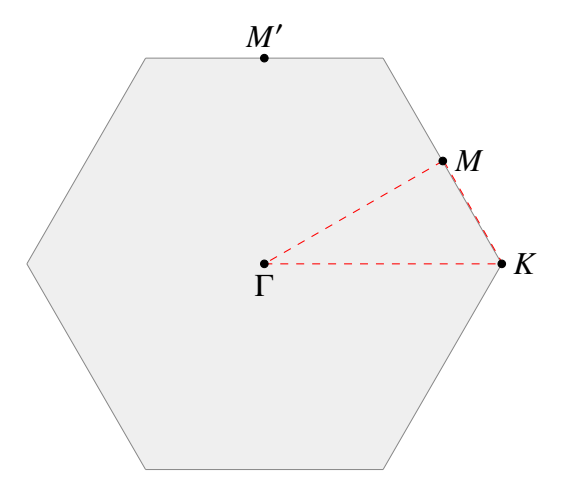


Figure 11: First Brillouin zone of the two-dimensional hexagonal lattice. It has the shape of a regular hexagon. The special points in \vec{q} -space have the following coordinates (q_x, q_y) : $\Gamma = (0, 0)$; $K = \frac{2\pi}{a}(\frac{2}{3}, 0)$; $M = \frac{2\pi}{a}(\frac{1}{2}, \frac{1}{2\sqrt{3}})$; $M' = \frac{2\pi}{a}(0, \frac{1}{\sqrt{3}})$.

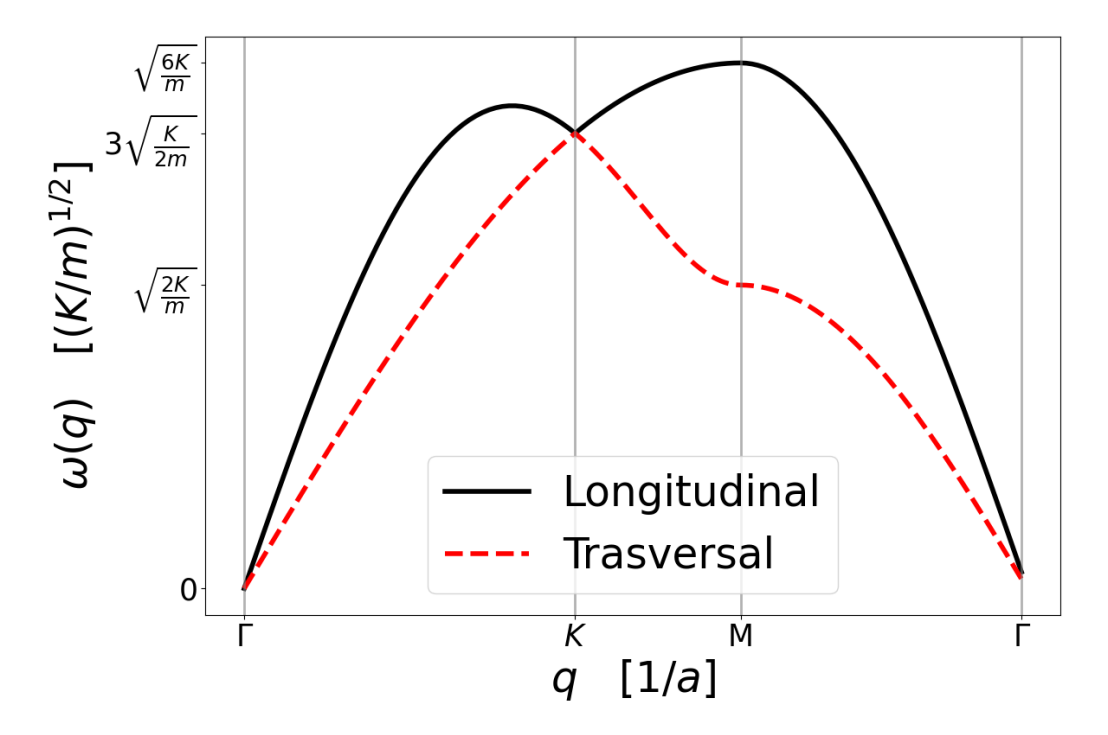


Figure 12: Hexagonal lattice phonon dispersion curves along the high-symmetry directions in the 1stBZ sketched in Figure 11. Only nearest-neighbors interaction is taken into account (K' = 0). The sound velocity isotropy manifests itself in the identical slope at Γ while arriving from different directions.

3 Third-Order Taylor Expansions

Taking advantage of the calculations made in Appendix B, we derive term V_3 in the expansion of the total potential of Eq.(1). The result for the square lattice, with reference to Figure 4 for the labelling of neighbour atoms j, is:

$$V_{3} = \frac{1}{6} \sum_{i=1}^{N} \left\{ \frac{2K}{a} \left[\sum_{j=1}^{2} (-1)^{j} \left(-u_{x_{j}} u_{y_{i}}^{2} - 2u_{y_{j}} u_{x_{i}} u_{y_{i}} + \frac{1}{2} u_{y_{j}}^{2} u_{x_{i}} + u_{x_{j}} u_{y_{j}} u_{y_{i}} \right) + \right.$$

$$\left. + \sum_{j=3}^{4} (-1)^{j} \left(-u_{y_{j}} u_{x_{i}}^{2} - 2u_{x_{j}} u_{x_{i}} u_{y_{i}} + \frac{1}{2} u_{x_{j}}^{2} u_{y_{i}} + u_{x_{j}} u_{y_{j}} u_{x_{i}} \right) \right] +$$

$$\left. + \frac{K'}{2a} \sum_{j=5}^{8} \left[(-1)^{j} \left(-3u_{y_{j}} u_{y_{i}}^{2} + u_{y_{j}} u_{x_{i}}^{2} + 2u_{x_{j}} u_{x_{i}} u_{y_{i}} + \frac{3}{2} u_{y_{j}}^{2} u_{y_{i}} - \frac{1}{2} u_{x_{j}}^{2} u_{y_{i}} - u_{x_{j}} u_{y_{j}} u_{x_{i}} \right) +$$

$$\left. + \left(\left(\frac{2j-13}{2} \right)^{2} - \frac{5}{4} \right) \left(3u_{x_{j}} u_{x_{i}}^{2} - u_{x_{j}} u_{y_{i}}^{2} - 2u_{y_{j}} u_{x_{i}} u_{y_{i}} - \frac{3}{2} u_{x_{j}}^{2} u_{x_{i}} + \frac{1}{2} u_{y_{j}}^{2} u_{x_{i}} + u_{x_{j}} u_{y_{j}} u_{y_{i}} \right) \right] \right\},$$

$$(22)$$

where $\left(\frac{2j-13}{2}\right)^2 - \frac{5}{4}$ is a "sign rule", i.e. it takes value ± 1 depending on j.

The third-order term for the hexagonal geometry, referring to Figure 9 for the

numbering of the neighbouring atoms j, is:

$$V_{3} = \frac{1}{6} \sum_{i=1}^{N} \left\{ \frac{K}{a} \sum_{j=1}^{2} (-1)^{j} \left(-4u_{y_{j}}u_{x_{i}}u_{y_{i}} - 2u_{x_{j}}u_{y_{i}}^{2} + u_{y_{j}}^{2}u_{x_{i}} + 2u_{x_{j}}u_{y_{j}}u_{y_{i}} \right) + \right.$$

$$+ \frac{K}{2a} \sum_{j=3}^{6} \left[\left(\left(\frac{2j-9}{2} \right)^{2} - \frac{5}{4} \right) \left(\frac{9}{2}u_{x_{j}}u_{x_{i}}^{2} - 5u_{y_{j}}u_{x_{i}}u_{y_{i}} - \frac{5}{2}u_{x_{j}}u_{y_{i}}^{2} - \frac{9}{4}u_{x_{j}}^{2}u_{x_{i}} + \frac{5}{4}u_{y_{j}}^{2}u_{x_{i}} + \frac{5}{2}u_{x_{j}}u_{y_{j}}u_{y_{i}} \right) +$$

$$+ \sqrt{3} \left(\frac{9/2-j}{|9/2-j|} \right) \left(\frac{3}{2}u_{y_{j}}u_{y_{i}}^{2} + u_{x_{j}}u_{x_{i}}u_{y_{i}} + \frac{1}{2}u_{y_{j}}u_{x_{i}}^{2} - \frac{3}{4}u_{y_{j}}^{2}u_{y_{i}} - \frac{1}{4}u_{x_{j}}^{2}u_{y_{i}} - \frac{1}{2}u_{x_{j}}u_{y_{j}}u_{x_{i}} \right) \right] +$$

$$+ \frac{K'}{\sqrt{3}a} \sum_{j=7}^{8} \left(-1 \right)^{j} \left(-4u_{x_{j}}u_{x_{i}}u_{y_{i}} - 2u_{y_{j}}u_{x_{i}}^{2} + u_{x_{j}}^{2}u_{y_{i}} + 2u_{x_{j}}u_{y_{j}}u_{x_{i}} \right) +$$

$$+ \frac{K'}{2a} \sum_{j=9}^{12} \left[\left(\left(\frac{2j-21}{2} \right)^{2} - \frac{5}{4} \right) \left(\frac{3}{2}u_{x_{j}}u_{x_{i}}^{2} + u_{y_{j}}u_{x_{i}}u_{y_{i}} + \frac{1}{2}u_{x_{j}}u_{y_{j}}^{2} - \frac{3}{4}u_{x_{j}}^{2}u_{x_{i}} - \frac{1}{4}u_{y_{j}}^{2}u_{x_{i}} - \frac{1}{2}u_{x_{j}}u_{y_{j}}u_{y_{i}} \right) +$$

$$+ \frac{1}{\sqrt{3}} \left(\frac{21/2-j}{|21/2-j|} \right) \left(\frac{9}{2}u_{y_{j}}u_{y_{i}}^{2} - 5u_{x_{j}}u_{x_{i}}u_{y_{i}} - \frac{5}{2}u_{y_{j}}u_{x_{i}}^{2} - \frac{9}{4}u_{y_{j}}^{2}u_{y_{i}} + \frac{5}{4}u_{x_{j}}^{2}u_{y_{i}} + \frac{5}{2}u_{x_{j}}u_{y_{j}}u_{x_{i}} \right) \right] \right\}.$$
(23)
In this expression
$$\left(\frac{2j-9}{2} \right)^{2} - \frac{5}{4}, \frac{9/2-j}{|9/2-j|}, \left(\frac{2j-21}{2} \right)^{2} - \frac{5}{4}, \text{ and } \frac{21/2-j}{|21/2-j|} \text{ are sign rules.}$$

4 Expansion Verification

In this section a MD code, which simulates the previously described systems and calculates V_{tot} , namely a numerical evaluation of the potential in Eq.(1), is exploited to verify if the Taylor expansion terms obtained in Sections 2 and 3 are correct.

In order to confirm the correctness of the V_2 and V_3 expressions, we conduct a few tests. We fix the initial pattern of deviations from equilibrium once and for all. In particular, we set an array $\tilde{\eta}$ that contains information about the initial displacements from equilibrium of all atoms. For example, we randomly choose such deviations in the [-0.5, 0.5] interval. Each displacement is then scaled by a factor α , a small length: usually $|\alpha| \ll a$.

In order to give a precise meaning to α , the array $\vec{\tilde{\eta}}$ of the starting displacements of dimension 2N is normalized:

$$\vec{\eta} = \frac{\vec{\tilde{\eta}}}{\|\vec{\tilde{\eta}}\|} \,\,, \tag{24}$$

where $\|\vec{\tilde{\eta}}\| = \sqrt{\sum_{i=1}^{2N} \tilde{\eta}_i^2}$. Now $\vec{\eta}$ is a dimensionless array of unit norm, while α is a length, that we can express in units of the lattice constant a.

We use the Bravais-lattice vector \vec{R}_i to identify the equilibrium position of the *i*-th atom. The starting deviations from the equilibrium configuration will be described by:

$$\vec{u}_0 = \alpha \, \vec{\eta} \ . \tag{25}$$

For both geometries, square and hexagonal, periodic boundary conditions (PBCs) are applied to a supercell: for the square lattice we take a $(6a \times 6a)$ supercell that

contains N=36 atoms; for the hexagonal crystal the supercell is $(6a \times 3\sqrt{3}a)$ in size, and contains N=36 atoms too.

For each α , we record the values of V_{tot} , V_2 , V_3 , in order to verify the following leading α dependences:

- $V_{\rm tot} \approx V_2 \propto \alpha^2$;
- $\Delta V_2 \equiv V_{\text{tot}} V_2 \approx V_3 \propto \alpha^3$;
- $\Delta V_3 \equiv V_{\text{tot}} V_2 V_3 \propto \alpha^4$, for $\alpha \to 0$.

4.1 Second-Order Terms

We first verify that the expressions in Eq.(13) and (19) are correct, by comparing V_2 and V_{tot} , plotted as a function of α^2 in Figure 13. We observe that the two quantities are practically coinciding, since, for small α , V_2 is the dominant term of the expansion. As shown in the insets, where a broader range in α is explored, for large displacements $\alpha \simeq a$, small deviations occur.

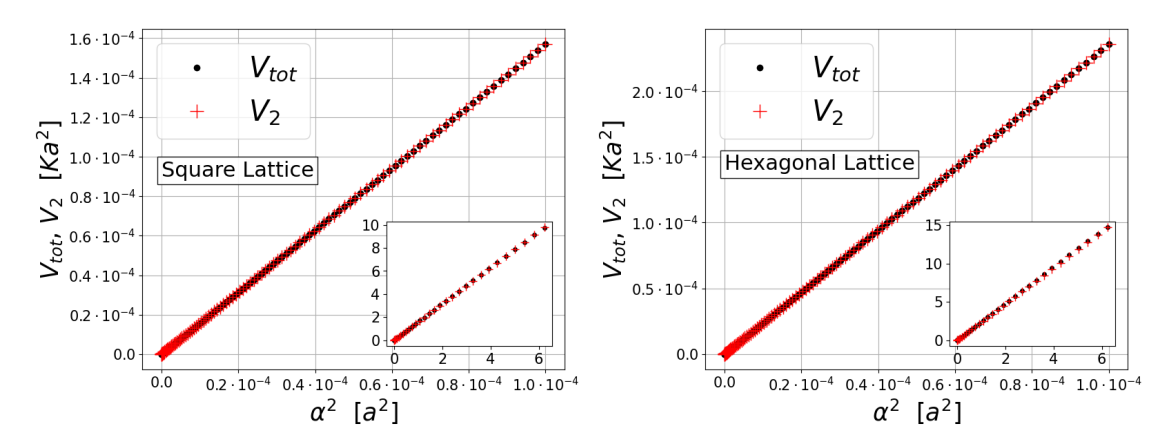


Figure 13: Comparison between the second-order Taylor term V_2 and the exact numerical value of V_{tot} , obtained for a fixed random displacement of unit norm, multiplied by an amplitude α , and reported as a function of α^2 . Since V_2 is the leading term in the expansion, for both geometries in the limit $\alpha \to 0$ these quantities coincide. The inset shows that deviations, representing anharmonic terms, are quite small even for displacements α of the order of α and even larger.

4.2 Third-Order Terms

A similar procedure is applied to the third-order terms V_3 , Eqs.(22) and (23), which are compared with the totality of the anharmonic terms $\Delta V_2 = V_{\rm tot} - V_2$. Figure 14 shows that in the limit $\alpha \to 0$ these two quantities coincide, so the expressions (22) and (23) are also validated. The prefactor of the α^3 term, and even its sign, depends on the specific initial configuration, which is picked in the choice of the random displacements. Also in this test, for large $\alpha \simeq a$, sizable deviations occur (see insets).

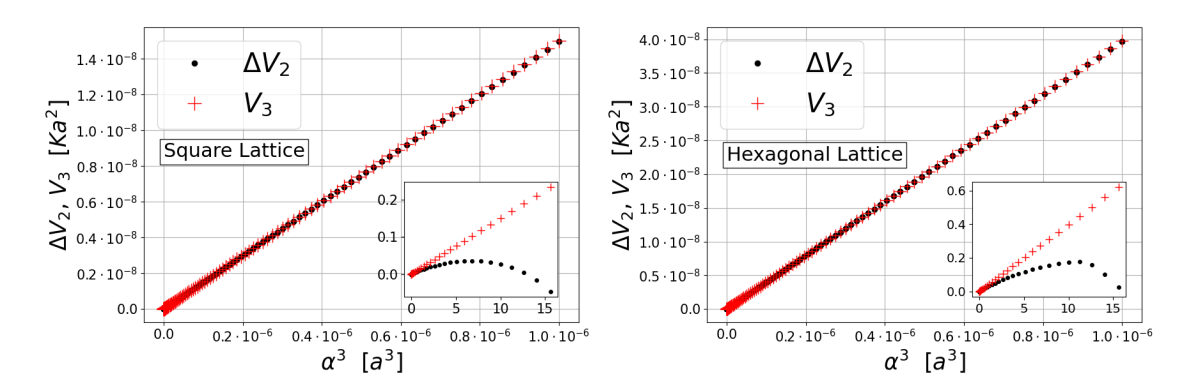


Figure 14: Comparison of the third-order term V_3 , computed according to Eq.(22) (square lattice, left) and (23) (hexagonal lattice, right), with $\Delta V_2 = V_{\text{tot}} - V_2$. The good agreement for small α indicates the correctness of the expressions obtained. The disagreement between ΔV_2 and V_3 observed for larger $\alpha \simeq a$ (insets) is due to the former containing terms of order higher than the third.

4.3 Higher-Order Terms

As a final check, in Figure 15 we verify that the leading contribution to the remainder $\Delta V_3 = V_{\rm tot} - V_2 - V_3$ is proportional to α^4 for small α . As expected, for $\alpha \gtrsim 1$ deviations appear, see insets.

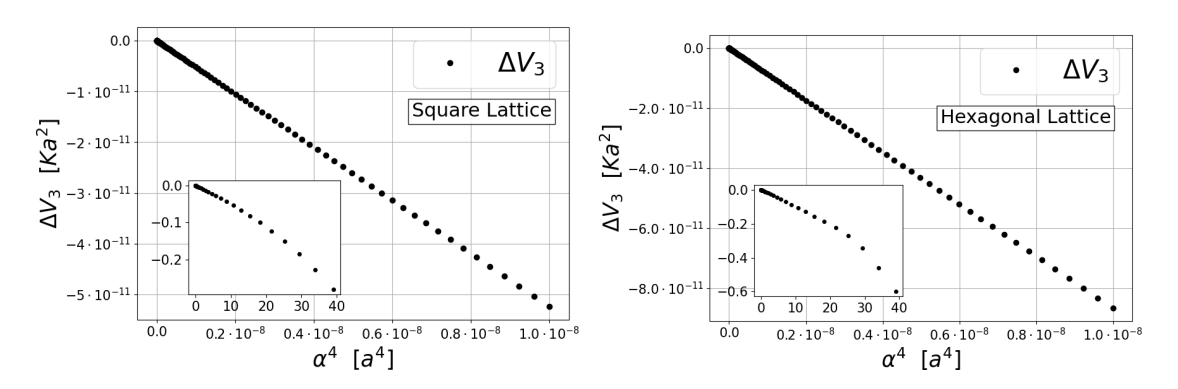


Figure 15: The remainder of the expansion truncated to third order, namely $\Delta V_3 = V_{\text{tot}} - V_2 - V_3$, exhibits a leading α^4 dependence for $\alpha \to 0$.

5 Numerical Simulations

We now proceed to investigate the effect of the geometric anharmonicity on the dynamics. The MD code integrates the equation of motion³ for the atoms in the crystal, obtaining a numerically accurate time evolution of the positions \vec{r}_i for i = 1, ..., N over

³The code adopts the Runge-Kutta-Fehlberg (RKF) method to integrate the resulting system of differential equations, with an adaptive time step to guarantee an accurate integration.

a predetermined time interval. Based on these dynamic variables, the code numerically estimates the time evolution of V_{tot} . J. Miglio [2] implemented a function to compute V_2 according to Eq.(13) for the square lattice. We added three new functions: one to calculate V_2 for the hexagonal crystal, Eq.(19); and two more functions that compute V_3 in both geometries, Eqs.(22) and (23).

The dynamics of the system is purely Newtonian, it includes no dissipative terms. We checked that the total energy is well conserved as it should. We simulate the two systems, square and hexagonal, within the two supercells introduced in Section 4, applying PBCs appropriately.

By default we run simulations with duration $t_{\rm end} = 30\sqrt{m/K}$. At the initial time $t_0 = 0$ a suitable starting configuration (not necessarily involving random displacements) is set. As in Section 4 all atoms have a starting displacement $\vec{u}_0 = \alpha \vec{\eta}$ and zero velocity. Therefore, initially the kinetic energy vanishes, and the potential energy is maximum.

To evaluate the time-averaged magnitude of $\Delta V_2 = V_{\rm tot} - V_2$, containing all anharmonic terms from the third order onward, we consider the following mean square:

$$\sigma_{\Delta V_2} = \left(\frac{\int_{t_0}^{t_{\text{end}}} \Delta V_2(t)^2 dt}{t_{\text{end}}}\right)^{\frac{1}{2}}.$$
 (26)

We evaluate $\sigma_{\Delta V_2}$ on a set of simulations all of the same duration, but characterized by different amplitudes α of the initial displacement. We report $\sigma_{\Delta V_2}(\alpha)$ on a bilogarithmic-scale graph. In this type of graph, a power law manifests itself in a linear trend, whose slope gives the exponent of the underlying power law. The resulting exponent provides information about which anharmonic term dominates in that specific phonon excitation.

This study on $\sigma_{\Delta V_2}$ was done by J. Miglio [2] for the square lattice. In the present thesis we have the possibility to study the new average magnitude

$$\sigma_{\Delta V_3} = \left(\frac{\int_{t_0}^{t_{\text{end}}} \Delta V_3(t)^2 dt}{t_{\text{end}}}\right)^{\frac{1}{2}},\tag{27}$$

of the deviation $\Delta V_3 = V_{\text{tot}} - V_2 - V_3$ that contains all anharmonic terms from the fourth order onward.

Since ΔV_3 values calculated by the RKF method at different instants of integration of differential equations are correlated within a certain correlation time, we cannot compute the standard deviation of $\sigma_{\Delta V_3}$ using the usual formula, because the time average under square root (27) is calculated on sampled values that are not independent. Therefore, in Appendix C we explain how we estimate $\sigma_{\Delta V_3}$ and its error.

Given a general equilibrium lattice vector $\vec{R} = n\vec{a_1} + m\vec{a_2}$ with $n, m \in Z$, a generic phonon wave has the form

$$\vec{\eta}(\vec{R}_i) = \vec{A}e^{i\vec{q}\cdot\vec{R}_i} , \qquad (28)$$

where $\vec{A} = (A_x, A_y)$ is the wave polarization vector. For simplicity, instead of studying propagating waves like the one in Eq.(28), we simulate stationary waves. In practice, we

take the real part of Eq.(28) and thus we excite the stationary modes of oscillation of the lattice, by fixing specific values of \vec{q} and of \vec{A} in the cosine expression:

$$\vec{\eta}(\vec{R}_i) = \vec{A}\cos(\vec{q} \cdot \vec{R}_i) \ . \tag{29}$$

We normalize the array $\vec{\eta}$ as detailed in Section 4.

5.1 Square Lattice

Different oscillation modes of the square lattice are simulated below. Since simulations deal with a 6×6 supercell, to which PBCs are applied, there are only discrete allowed \vec{q} points in the first Brillouin zone, determined by the following rule [3]:

$$\vec{q} = \frac{n_1}{N_{n_1}} \vec{b}_1 + \frac{n_2}{N_{n_2}} \vec{b}_2 , \qquad (30)$$

where

$$n_{\xi} = -\frac{N_{n_{\xi}}}{2} + 1, -\frac{N_{n_{\xi}}}{2} + 2, \dots, \frac{N_{n_{\xi}}}{2} - 2, \frac{N_{n_{\xi}}}{2} - 1, \frac{N_{n_{\xi}}}{2},$$

and $N_{n_{\xi}}$ are lattice repetitions in the \vec{a}_1 , \vec{a}_2 primitive directions. Since $N_{n_1} = N_{n_2} = 6$, the allowed \vec{q} points are:

$$q_x, q_y = 0, \pm \frac{1}{6} \frac{2\pi}{a}, \pm \frac{2}{6} \frac{2\pi}{a}, \frac{3}{6} \frac{2\pi}{a}.$$

Points with $q_x = -\frac{\pi}{a}$ and/or $q_y = -\frac{\pi}{a}$ are excluded because they coincide with $q_x = \frac{\pi}{a}$ and/or $q_y = \frac{\pi}{a}$ (zone-edge \vec{q} values).

This preliminary study shows that, because of the PBCs, there are $N_{n_1}N_{n_2} = 36$ allowed wavevectors in the 1stBZ and then 36 phonon modes per phonon branch. The total number of different phonon modes in the two branches is $2N_{n_1}N_{n_2} = 72$, coinciding with the number of degrees of freedom for the motion in 2D of $N_{n_1}N_{n_2} = 36$ atoms. We first simulate two different zone-edge (ZE) phonons, and then a random superposition of normal modes.

5.1.1 Point-X Zone-Edge Phonon

Longitudinal and transverse vibration waves of the square crystal with wavevector equal to $\vec{q} = \frac{\pi}{a}(1,0)$ have wavelength $\lambda = 2a$. They are located at the X simmetry point of Figure 5. According to Eq.(29), the initial displacements are:

$$\eta_{x_i} = \cos\left(\frac{\pi}{a}\vec{R}_i\right) , \qquad \eta_y = 0 .$$
(31)

 \vec{R}_i assumes the values of the equilibrium atomic positions $\vec{R}_i = i \cdot a$, where i = 0, 1, ..., 5. This pattern of displacements is illustrated in Figure 16.

The $\sigma_{\Delta V_2}$ study conducted in Ref.[2] concluded that, for both longitudinal and transverse phonons at X, the dominant anharmonic term in the $\alpha \to 0$ limit is the fourth, since the third order cancels out. The justification given for the fact that $V_3 = 0$ can be found in Ref.[2]'s Appendix and goes as follows: "the third order is a combination

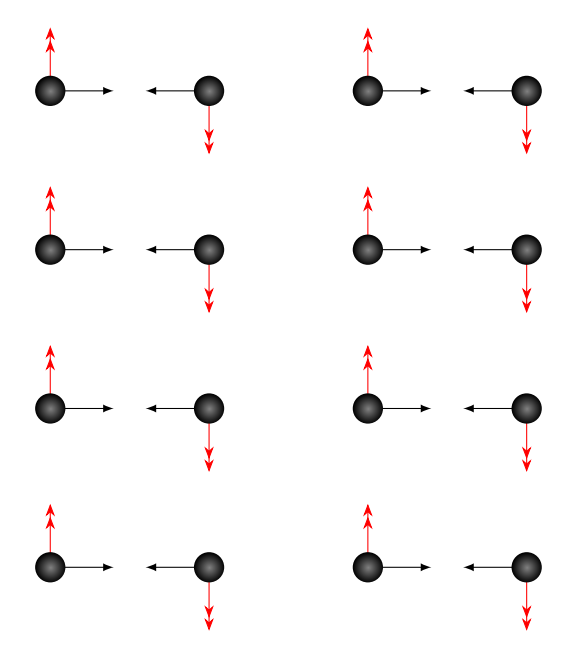


Figure 16: Point-*X* zone-edge atomic initial displacements. The normal mode wavelength is $\lambda = \frac{2\pi}{q} = 2a$. Black single arrows describe the longitudinal phonon; red double arrows represent the transverse motion.

of polynomials coupled in such a way that their total sum cancels out as a result of displacements from the equilibrium position that follow the symmetries of the lattice under consideration". That statement can now be confirmed by examining Eq.(22): taking longitudinal motion as an example, all terms $\propto u_{y_{i/j}}$ vanish: therefore only the terms $\propto \alpha u_{x_j} u_{x_i}^2$ and $\propto \alpha u_{x_j}^2 u_{x_i}$ could be nonzero. However, by adding all these terms up, taking into account the appropriate signs, they cancel each other out.

Figure 17 reports the time evolution of ΔV_2 and ΔV_3 for both longitudinal and transverse waves, excited with a small amplitude $\alpha=10^{-2}a$. Since $V_3=0$, ΔV_2 and ΔV_3 coincide. The amplitude of these high-order energy terms is larger for the transverse mode than for the longitudinal one. The oscillations have different frequencies, that match Figure 7. Figure 18 reports the average magnitudes of $\sigma_{\Delta V_2}$ and $\sigma_{\Delta V_3}$ as a function of α . Of course, $\sigma_{\Delta V_2}$ coincides with $\sigma_{\Delta V_3}$ for both longitudinal and transverse phonons. A logarithmic fit of the data reveals a power law of the type: $\sigma_{\Delta V_3} \propto \alpha^4$. This means that the dominating term is the fourth-order one, since $V_3=0$. Error bars are visible and represent the fluctuations associated with each $\sigma_{\Delta V_2}(\alpha)$ or $\sigma_{\Delta V_3}(\alpha)$ point. Here and in the rest of this thesis, they are estimated using Eq.(48). Incompatibility between the expected and estimated angular coefficient is observed in Figure 18. Compatible values are obtained by repeating the study on a smaller number of $\sigma_{\Delta V_3}$ points.

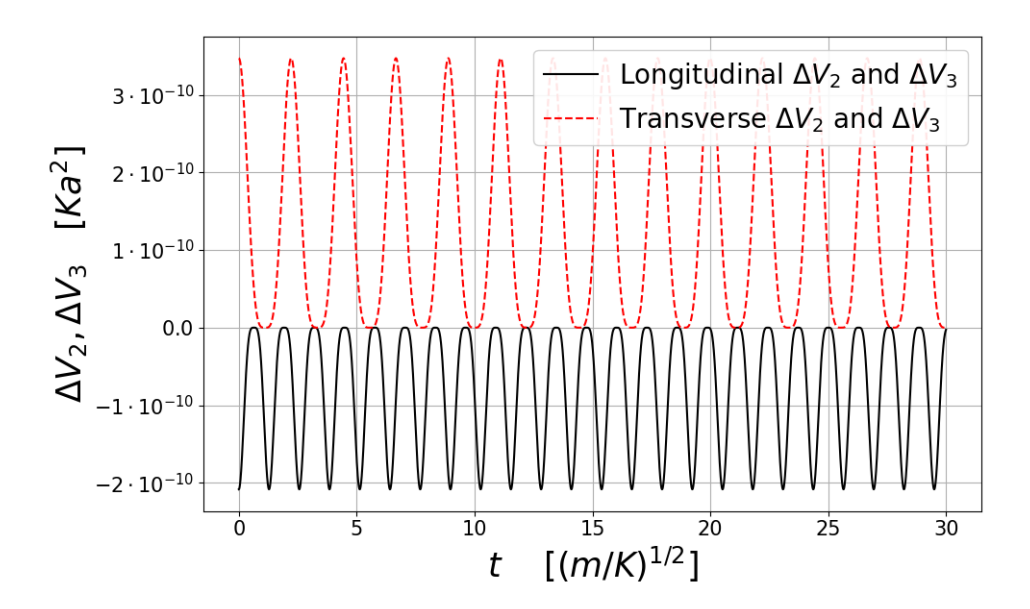


Figure 17: Time evolution of ΔV_2 and ΔV_3 (coincident) for the longitudinal (black solid line) and transverse (red dashed line) phonon excitations at the \vec{q} point X of a 6×6 square lattice. The excitation amplitude is $\alpha = 10^{-2}a$. The longitudinal motion is associated to a higher-oscillation frequency and a smaller amplitude of these anharmonic terms.

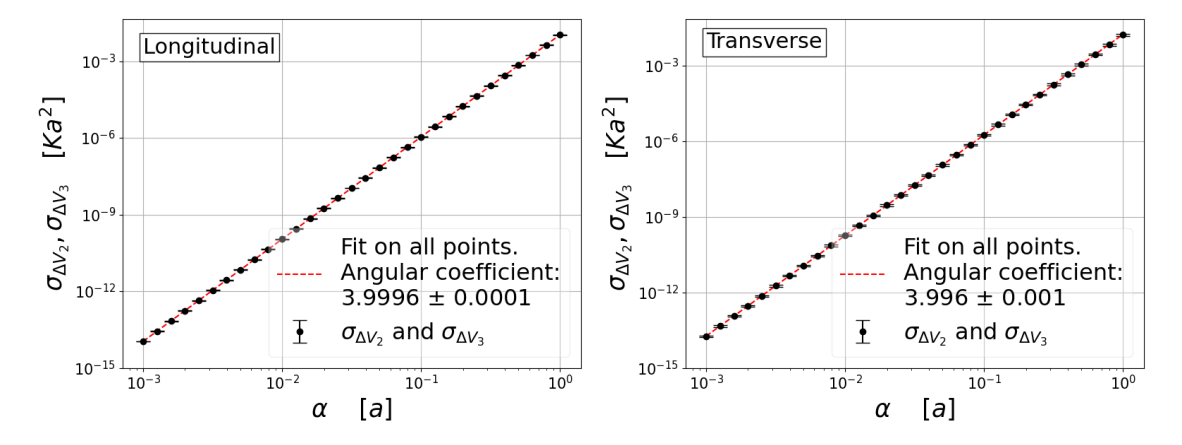


Figure 18: $\sigma_{\Delta V_2}(\alpha)$ and $\sigma_{\Delta V_3}(\alpha)$, Eqs.(26) and (27), for the ZE longitudinal and transverse phonons at X for the square lattice (see Figures 5 and 16). Both follow a power law $\sigma_{\Delta V_3} \propto \alpha^4$ over a broad range of α , as confirmed by a linear fit on the logarithms of α and $\sigma_{\Delta V_3}$, whose angular coefficients are compatible with the expected exponent 4. Error bars represent the fluctuations related to the calculation of $\sigma_{\Delta V_3}$ and they are estimated using Eq.(48). Each point is the result of an average over a simulation of duration $t_{\rm end} = 30 (m/K)^{1/2}$.

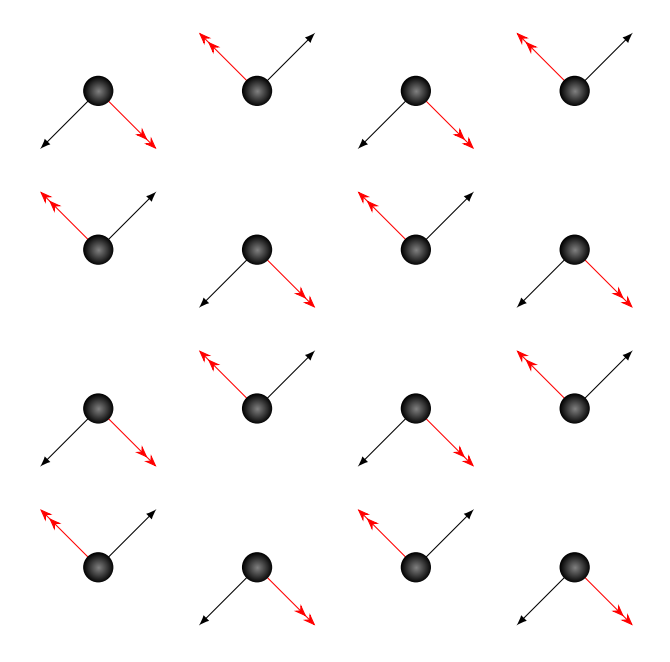


Figure 19: Diagonal ZE atomic displacements. Black single arrows describe longitudinal displacements; red double arrows represent transverse displacements for $\vec{q} = \frac{2\pi}{a}(1,1)$. The two are interchangeable if we consider the equivalent point $\vec{q} = \frac{2\pi}{a}(1,-1)$.

5.1.2 Point-M Zone-Edge Phonon

Next, we simulate zone-edge phonons at the 1stBZ corner, i.e. oscillations having wavevector $\vec{q} = \frac{\pi}{a}(1,1)$, namely the M point in Figure 5, with wavelength $\lambda = \frac{2\pi}{|\vec{q}|} = \sqrt{2}a$. Figure 19 visualizes the atomic starting displacements.

Figure 19 makes it clear that, at this \vec{q} point in practice the longitudinal motion is equivalent to the transverse one. This observation is reflected in the fact that the respective phonon dispersion frequencies coincide at the M point in Figure 7 and that $\Delta V_2(t)$ and $\Delta V_3(t)$ coincide in Figure 20, which shows the time evolution of ΔV_2 and ΔV_3 for $\alpha = 10^{-2}a$.

As in the previous subsection, the trend of $\sigma_{\Delta V_3}$ as a function of α is studied. Figure 21 shows the results. For this diagonal ZE atomic oscillation, exactly as in the X-point phonon, the dominant anharmonic term is the fourth, since $V_3 = 0$.

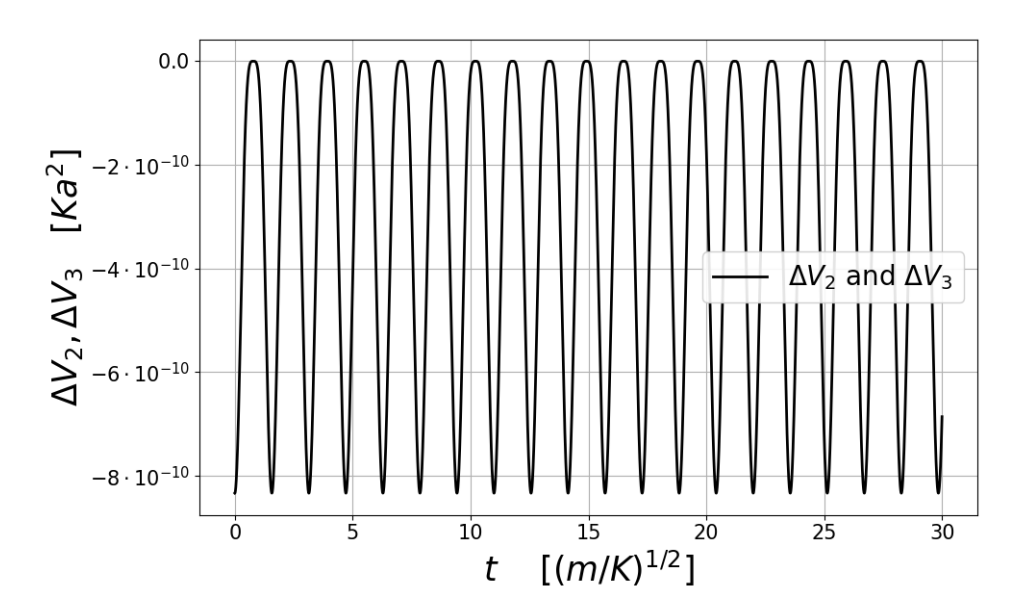


Figure 20: For $\alpha = 10^{-2}a$, perfectly coinciding ΔV_2 and ΔV_3 associated with ZE longitudinal or transverse phonons at M point of the hexagonal lattice. This quantity is systematically negative.

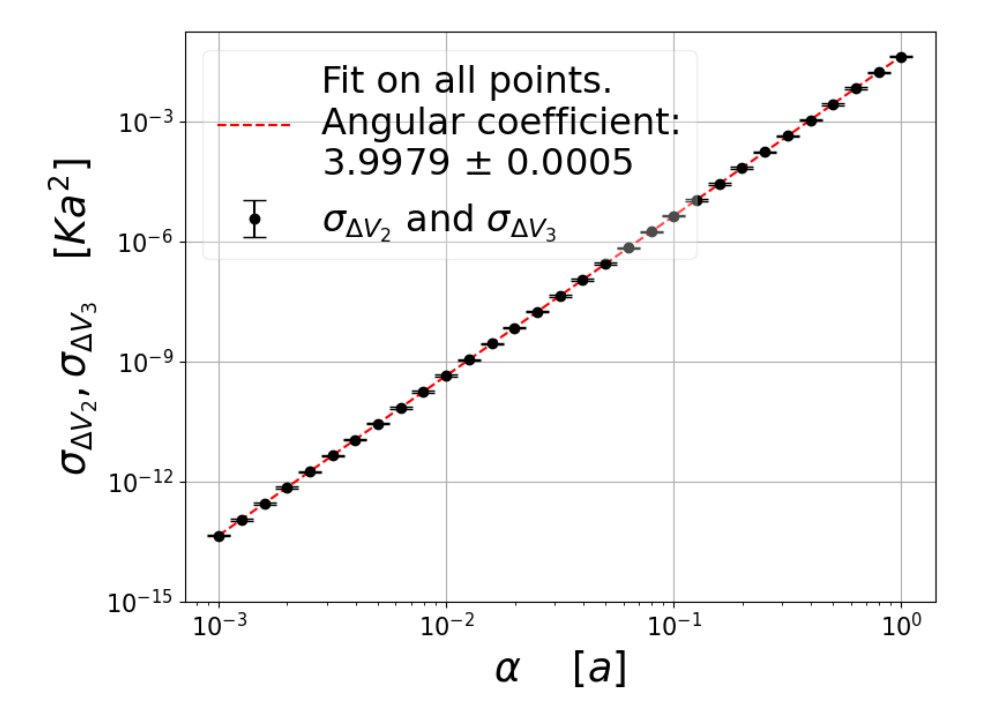


Figure 21: $\sigma_{\Delta V_3}$ as a function of the amplitude α of a $\vec{q} = M$ phonon excitation of a 6×6 square lattice. Like in Figure 18, a fit on data points confirms the power law $\sigma_{\Delta V_3} \propto \alpha^4$. Data points and their error bars are computed as in Figure 18. Longitudinal and transverse phonon frequencies coincide at point M.

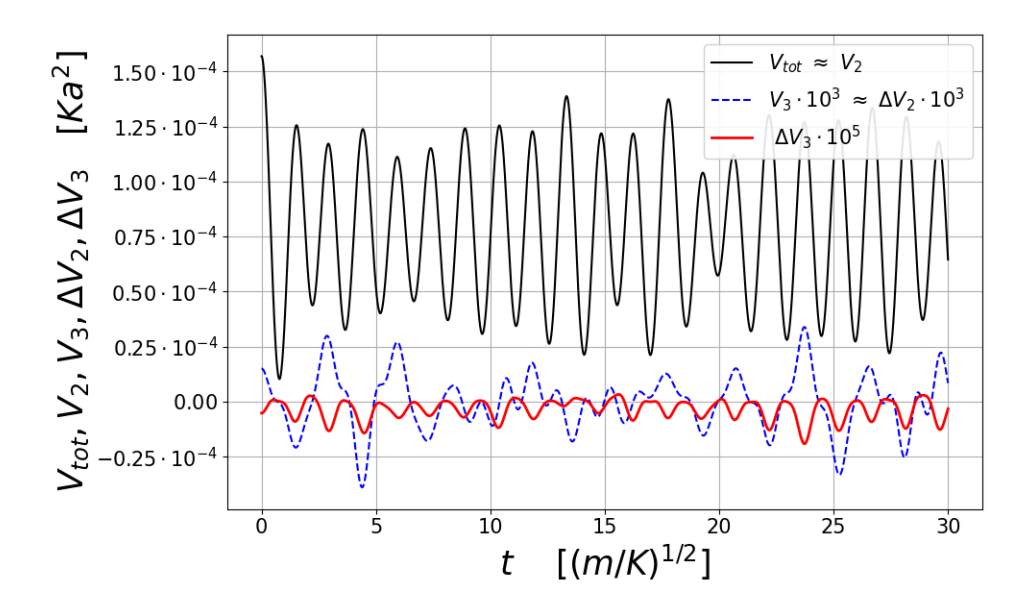


Figure 22: V_{tot} , V_2 , V_3 , ΔV_2 and ΔV_3 as a function of time, related to the random combination of phonons of the square lattice for $\alpha = 10^{-2}a$. Since V_{tot} and V_2 have much larger amplitude than the other quantities, we multiply V_3 and ΔV_2 by 10^3 , and ΔV_3 by 10^5 , in order for all the signals to be visible.

5.1.3 Combination Of Phonons

For all special displacements investigated so far, the V_3 term vanishes exactly. In contrast, by starting with random displacements from equilibrium, like for the static evaluations of Section 4, we can excite several phonon modes simultaneously and, as a result of the lack of symmetry, we can explore situations where $V_3 \neq 0$.

Figure 22 shows the time evolution of V_{tot} , V_2 , V_3 , ΔV_2 , ΔV_3 . These oscillations are the result of the superposition of vibrating modes of different frequencies and amplitudes. We can compare them, for example, with the single-mode oscillation in Figure 20.

Figure 23 illustrates the results of the average amplitude $\sigma_{\Delta V_3}$ analysis. In this simulation $V_3 \neq 0$ and then it is the leading anharmonic term; the next one is the fourth order.

5.2 Hexagonal Lattice

In the following we simulate different hexagonal crystal oscillations. In this case $N_{n_1} = 6$ and $N_{n_2} = 6$. Therefore, referring to Eq.(30):

$$n_1, n_2 = 0, \pm 1, \pm 2, 3$$

and there are $N_{n_1}N_{n_2} = 36$ allowed wavevectors in the 1stBZ as well as 36 phonon modes per branch. The number of degree of freedom and therefore the total number of phonon modes in the two branches is 72.

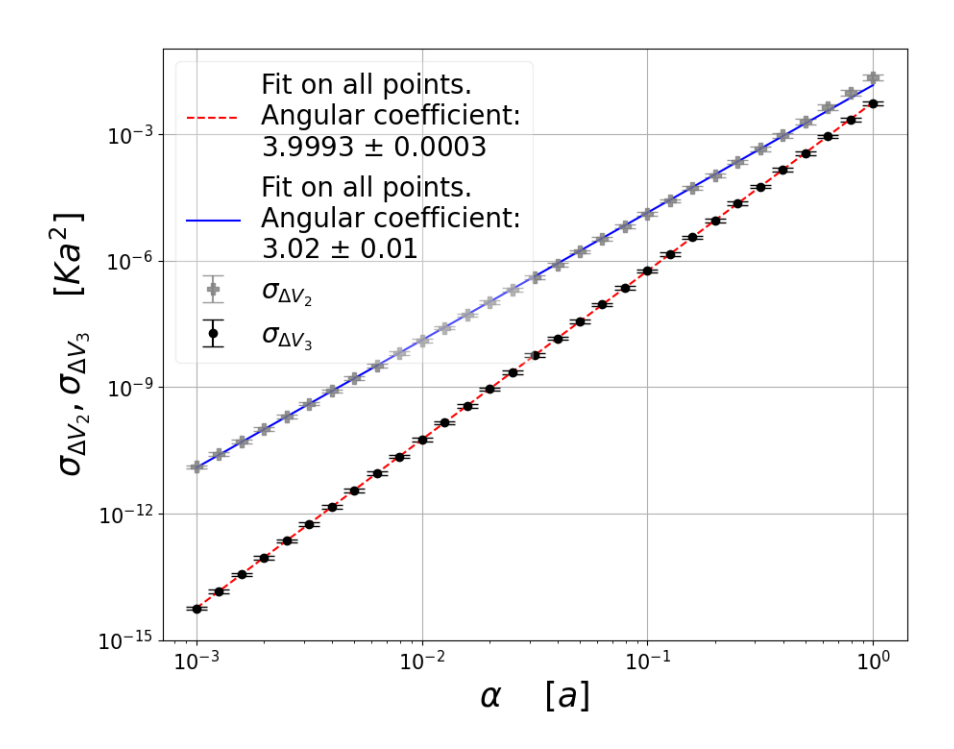


Figure 23: $\sigma_{\Delta V_2}$ and $\sigma_{\Delta V_3}$ for a random oscillation of the square lattice. Two distinct fits reveal that $\sigma_{\Delta V_2} \propto \alpha^3$, while $\sigma_{\Delta V_3} \propto \alpha^4$. Error bars are visible and they are computed using Eq.(48).

5.2.1 Point-*K* Zone-Edge Phonon

The ZE phonon associated with point K in Figure 11 has $\vec{q} = \frac{2\pi}{a} \left(\frac{2}{3}, 0 \right)$ and thus a wavelength $\lambda = \frac{3}{2}a$. According to the Eq.(29), the initial longitudinal displacements from equilibrium are:

$$\eta_{x_i} = \cos\left(\frac{4\pi}{3a}\vec{R}_i\right) , \qquad \eta_y = 0 ,$$
(32)

where \vec{R}_i assumes values which are integer multiples of a/2.

Figure 24 sketches the atomic displacements for this normal mode of oscillation. Exactly like for the ZE phonon at point M in the square lattice, also for this phonon of the hexagonal lattice the longitudinal and transverse motion coincide. We see the coincidence of these frequencies in Figure 12, where the respective dispersion curves meet at point K.

Figure 25 compares the time evolution of V_3 and ΔV_2 . By analysing Eq.(23), like we did for the square lattice, we see that V_3 vanishes for the initial displacements of this phonon. Indeed, in Figure 25 we observe that this happens at the beginning of the simulation. However, as soon as the system begins to vibrate, anharmonic terms are activated, which excite weakly some other phonon mode, whose coupling provides V_3 with the peculiar time evolution observed in Figure 25: three small peaks alternating with a larger one.

In Figure 26, we observe that V_{tot} and its Taylor terms from fourth order onward (i.e. ΔV_3) oscillate at the same frequency. However, ΔV_3 deviates visibly from the cosine-like profile of V_{tot} .

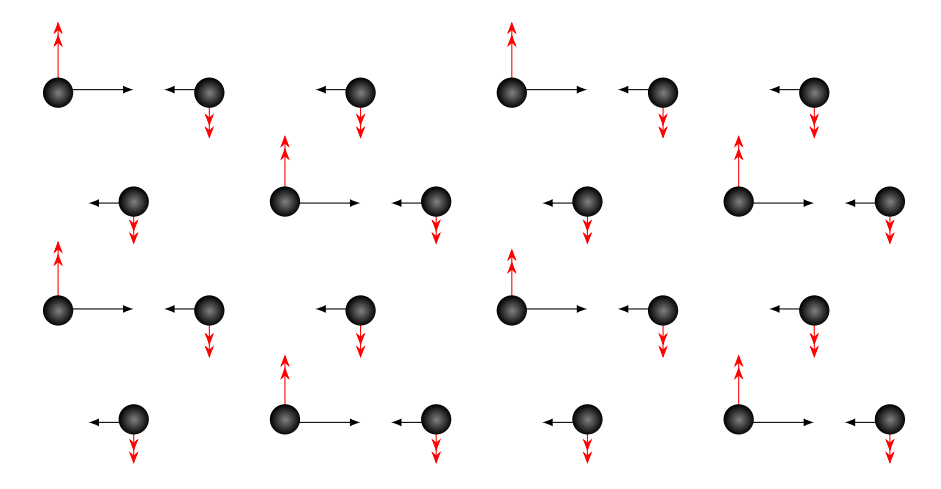


Figure 24: ZE phonon on point K of the hexagonal lattice. Black single arrows refer to longitudinal oscillation, red double ones instead describe the transverse phonon. The wavelength associated to this normal mode is $\lambda = \frac{3}{2}a$. Note that the shorter arrows have half the length of the longer ones and opposite orientation.

To evaluate the power law of V_3 energy contribution, we execute the average amplitude $\sigma_{\Delta V_2}$ and $\sigma_{\Delta V_3}$ analysis. Figure ?? exposes the results of this study. Remarkably, the fit on $\sigma_{\Delta V_3}$ data reveals that the fourth order is the dominant anharmonic one, like for the $\sigma_{\Delta V_2}$ points. The latter is of course dominated by fourth-order terms, $\sigma_{\Delta V_2} \propto \alpha^4$. The difference between ΔV_2 and ΔV_3 is similar to $\langle V_3 \rangle$. If we evaluated the quadratic mean of V_3 with an expression similar to Eq.(27), we would also obtain a power law $\propto \alpha^4$, which is quite remarkable for a third-order term.

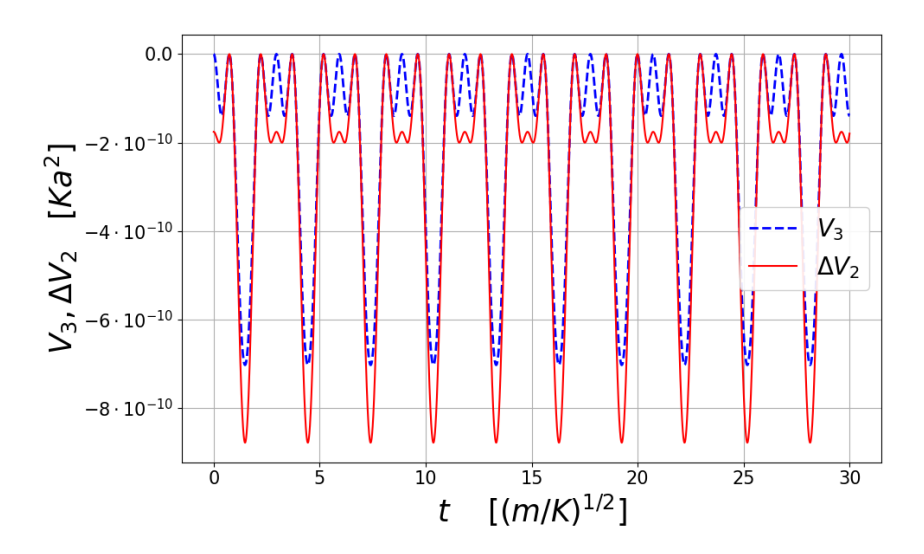


Figure 25: Third-order Taylor expansion (blue dashed line) compared with ΔV_2 (solid red line). These oscillations correspond to $\alpha = 10^{-2}a$. Longitudinal and transverse motion coincide for the specific point-K phonon of the hexagonal lattice (Figure 12). V_3 vanishes exactly at $t_0 = 0$, as predicted by Eq.(23). The observed time evolution originates because of anharmonic terms of higher-than-third order.

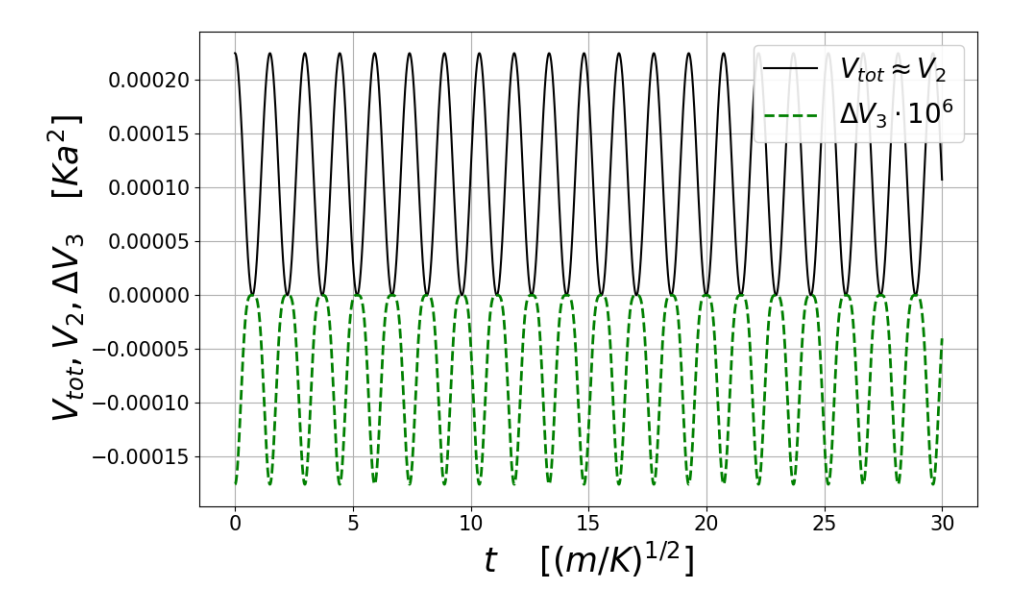


Figure 26: Terms from the fourth order onward (ΔV_3 , green dashed line), compared with the total potential (black solid line), for $\alpha = 10^{-2}a$ and the coinciding longitudinal and transverse oscillations at point K, for the hexagonal lattice. ΔV_3 is multiplied by 10^6 in order to make it visible.

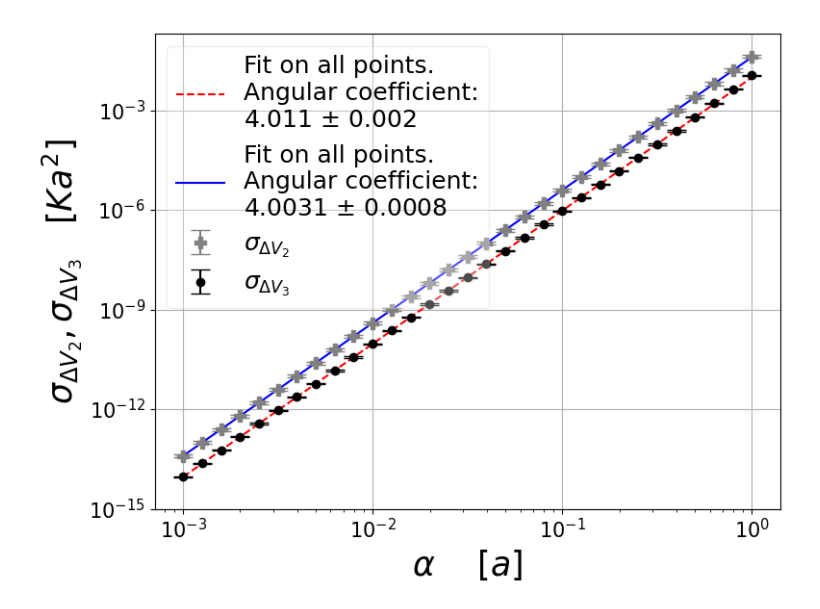


Figure 27: Zone-edge phonons at point K of the hexagonal lattice, see Figure 11. Longitudinal and transverse waves coincide as shown in Figure 12. $\sigma_{\Delta V_2} \propto \alpha^4$ and $\sigma_{\Delta V_3} \propto \alpha^4$. However, there is a difference in the prefactor of the power laws, which translates in a shift of the two linear trends in log scale. This is due to the fact that, even if $V_3 = 0$ at t_0 , however, once the system starts to vibrate, other phonons are weakly activated and their coupling provides an energy contribution of third order in the displacements, see Figure 25. These other modes are responsible for $\sigma_{\Delta V_2} \propto \alpha^4$, but not coinciding with $\sigma_{\Delta V_3}$.

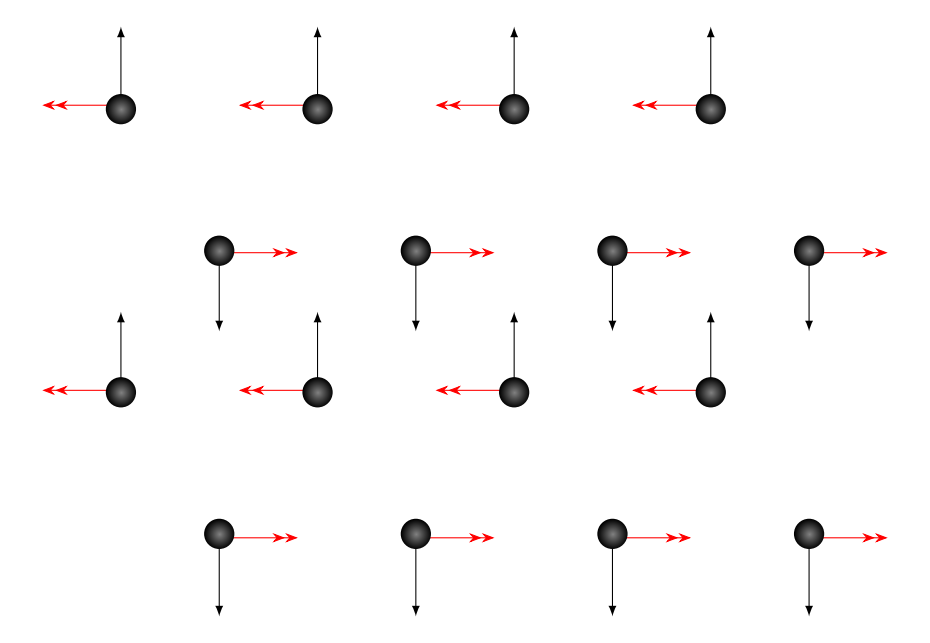


Figure 28: Zone-edge phonon at point M' of the hexagonal lattice, Figure 11. This wave has $\lambda = \sqrt{3}a$. Black single arrows identify the longitudinal displacement, while red double arrows describe the transverse one.

5.2.2 Point-M' Zone-Edge Phonon

Next, we simulate a zone-edge phonon at M' point of the hexagonal lattice, Figure 11. It has $\vec{q} = \frac{2\pi}{a}(0, \frac{1}{\sqrt{3}})$ and $\lambda = \sqrt{3}a$. Longitudinal displacements from equilibrium along the vertical direction are:

$$\eta_x = 0 , \qquad \eta_{y_i} = \cos(\frac{2\pi}{\sqrt{3}a}\vec{R}_i) ,$$
(33)

with $\vec{R}_i = \sqrt{3}a \cdot i$ and $i = 0, \frac{1}{2}, 1, \dots, \frac{5}{2}$. Figure 28 schematises the atomic initial displacements for this phonon.

In Figure 29 we report $\Delta V_2(t)$ and $\Delta V_3(t)$ for $\alpha = 10^{-2}a$. The two quantities coincide for both the longitudinal and the transverse motion. This suggests that $V_3 \equiv 0$. The two oscillations have visibly different frequencies, as expected at point M, see Figure 12.

In Figure 30 we evaluate the amplitude of the dominant anharmonic orders. What emerges is that $\sigma_{\Delta V_2} = \sigma_{\Delta V_3} \propto \alpha^4$ and then even for these modes the fourth order is the leading one.

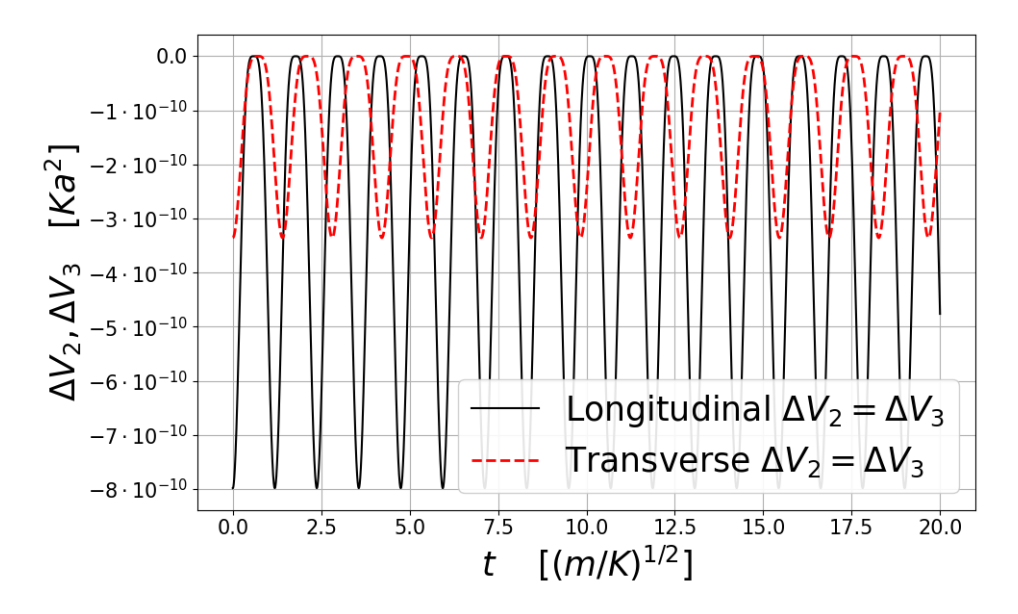


Figure 29: $\Delta V_2(t)$ and $\Delta V_3(t)$ associated with the longitudinal (black solid line) and transverse (red dashed line) ZE oscillation at point M' of the hexagonal lattice. They are computed for $\alpha = 10^{-2}a$. The two waves are different in amplitude and frequency.

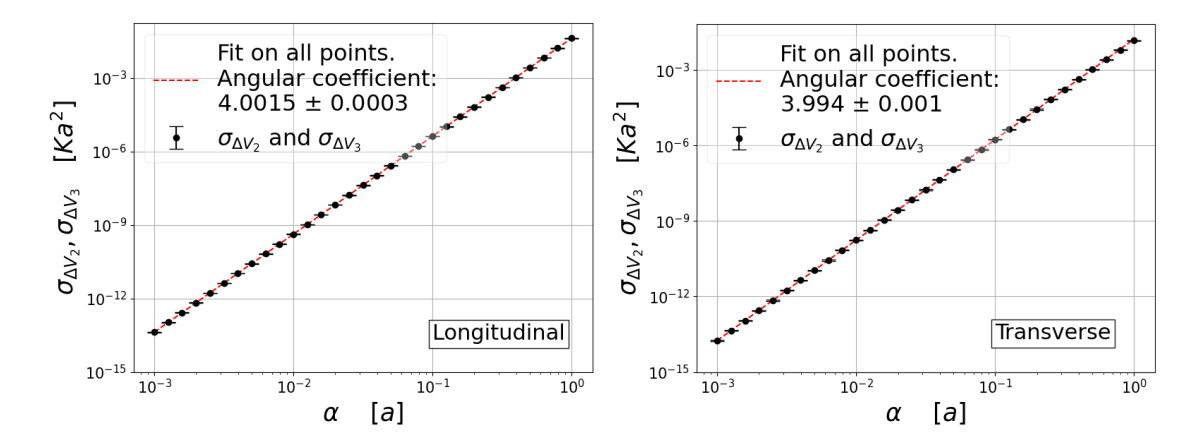


Figure 30: ZE phonon at point M' of the hexagonal lattice, Figure 11. The fit's slope reveals that $\sigma_{\Delta V_3} \propto \alpha^4$ for the longitudinal and for the transverse motion. Thus, as long as $V_3 = 0$, the fourth is the leading anharmonic order.

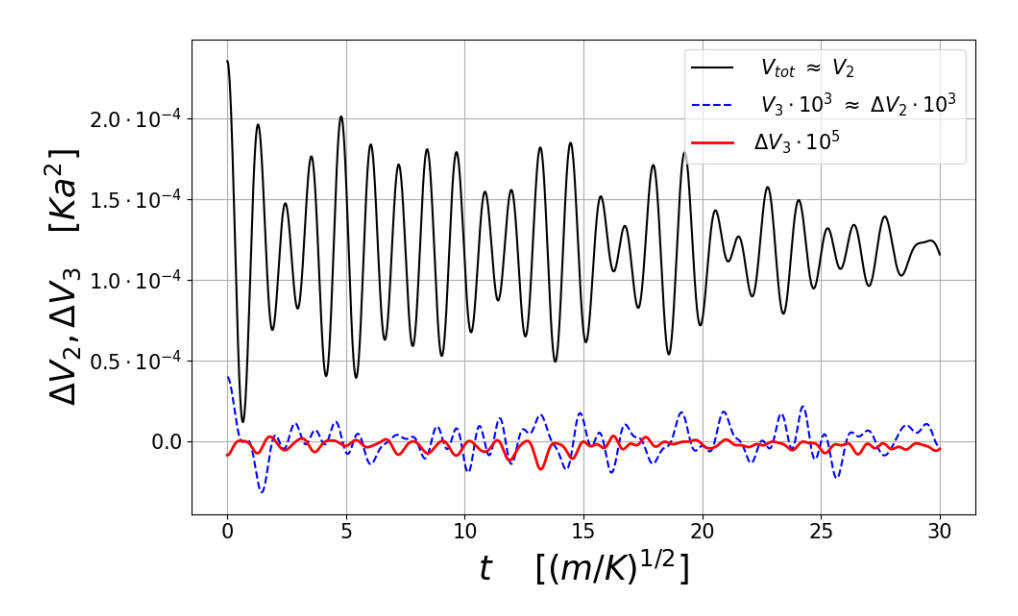


Figure 31: Time evolution of $V_{\text{tot}} \approx V_2$, V_3 , ΔV_2 and ΔV_3 for a random excitation with $\alpha = 10^{-2}a$ of the hexagonal lattice. We multiply V_3 and ΔV_2 by a factor 10^3 , and ΔV_3 by 10^5 for easier comparison.

5.2.3 Combination Of Phonons

By exciting the single phonon at high-symmetry point M', we observed that V_3 vanishes exactly. Also for the point-K phonon we concluded that $V_3 = 0$ at t_0 , by looking at Figure 25. However, the phonon at point K is characterised by the fact that, as soon as the atoms begin to move, other phonons emerge, whose coupling is responsible for the time evolution of V_3 in Figure 25.

In order to investigate an atomic motion with $V_3 \neq 0$ (even at t_0), we simulate a random superposition of vibrational modes of the hexagonal lattice, generated by random displacements, like in Section 5.1.3.

Figure 31 compares the time evolution of all the studied quantities for this random combination of phonons. As expected, these oscillations have no periodicity.

The time averages of Figure 32 reveal that the leading order of the anharmonic terms in V_{tot} is the third order, followed by the fourth one, as proved by $\sigma_{\Delta V_2} \propto \alpha^3$ and $\sigma_{\Delta V_3} \propto \alpha^4$.

6 Conclusions

In this thesis we have studied a few aspects of lattice dynamics and geometric anharmonicity. In particular, we have considered 2D crystal lattices of different geometry: square and hexagonal.

In Section 2 we have calculated the harmonic phonon dispersion frequencies for these systems. Then, with the intention of going beyond the harmonic approximation and investigating the nature of geometric anharmonicity, in Section 3 we have derived the expressions of the third-order terms in the Taylor expansion of the total potential in

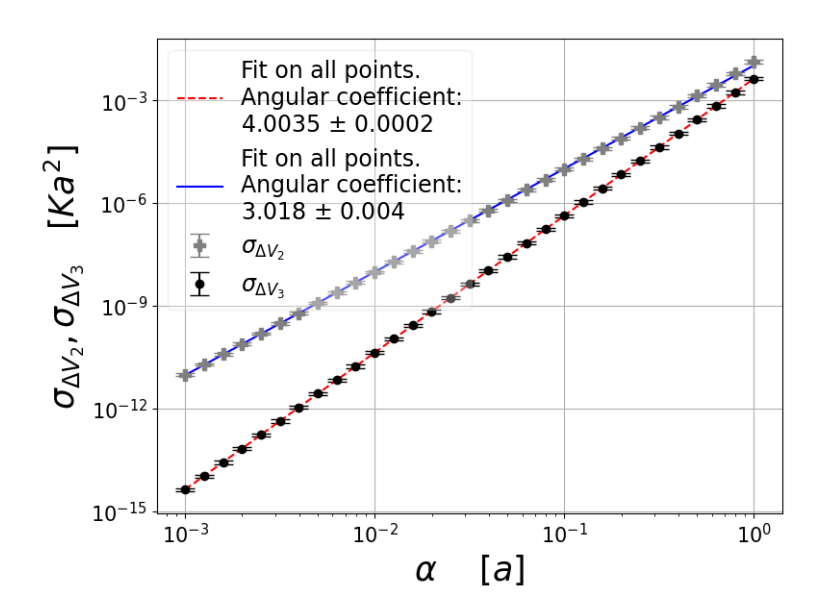


Figure 32: Study on dominant orders in a random superposition of phonons of the hexagonal lattice. Two fits reveal the power laws $\sigma_{\Delta V_2} \propto \alpha^3$ and $\sigma_{\Delta V_3} \propto \alpha^4$. Error bars are computed as explained in Appendix C.

Eq.(1), for both geometries. We have verified the correctness of these expressions in Section 4.

Finally, in Section 5 we have conducted a few numerical simulations using a MD code. For both bidimensional lattice geometries, we have first studied certain zone-edge single phonons, and then a combination of vibrating modes. For each of these atomic motions, we have analysed which terms of the Taylor expansion of V_{tot} dominate. In particular, we have executed a campaign of simulations, changing the vibration amplitude α and evaluating the average quantities $\sigma_{\Delta V_2}$ and $\sigma_{\Delta V_3}$, Eqs.(26) and (27). We have verified that for specific zone-edge phonons, associated with certain high-symmetry points, the third-order term vanishes and the fourth one is the leading anharmonic term. In the hexagonal crystal, however, we have identified a zone-edge phonon (point K, Figure 11) where $V_3 = 0$ only at the beginning of the simulation: during the time evolution, anharmonic terms activate other phonon modes, producing a nonzero V_3 whose average amplitude, remarkably, grows as α^4 . We have verified that the same phenomenon occur for other \vec{q} points, not at the zone boundary. A precise theoretical understanding of this peculiar coupling phenomenon probably deserves further attention.

When we excite a random set of phonons, V_3 is the first dominant anharmonic term, in both the square and hexagonal lattice. This is the expected behaviour for general displacements, where symmetry does not cancel third-order terms. Perhaps, a single phonon mode associated to nonzero V_3 may exist and it would be interesting to identify.

This research could also be extended by assuming a different pairwise interaction between atoms, e.g. a Lennard-Jones potential. One would need to replace the expression of this new potential in Eq.(42) and carry out a similar derivation to the one reported in Appendix B.

Another extension of the present work would be the calculation of the fourth-order

terms in the potential. This V_4 term would allow us to describe precisely anharmonicity even in simple high-symmetry single-phonon excitation. Besides, V_4 would permit us to study the new quantity $\Delta V_4 \equiv V_{\text{tot}} - V_2 - V_3 - V_4$, which contains all anharmonic terms starting from the fifth order.

Finally, it would be interesting to evaluate the effect of these anharmonic terms on the overall equation of state for such model crystal.

A Dynamical Matrix Method

We follow the method suggested by Ref.[7] to derive the phonon dispersion curves in harmonic approximation.

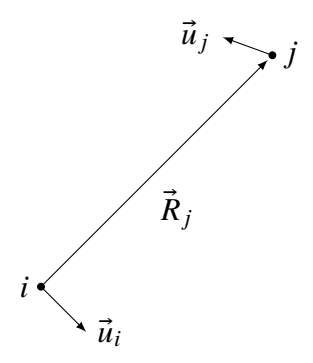


Figure 33: Diagram on the interaction between atom i and a j-th atom. In addition to the \vec{R}_j vector, which connects the positions of the two, generic displacement vectors \vec{u}_i and \vec{u}_j are also represented.

Referring to Figure 33, the central force that the atom i experiences when it interacts with the j-th atom is:

$$\vec{F}_{i} = K_{i} \left[\hat{R}_{i} \cdot (\vec{u}_{i} - \vec{u}_{i}) \right] \hat{R}_{i} , \qquad (34)$$

where $\hat{R}_j = \vec{R}_j/|\vec{R}_j|$ and \vec{u}_j , \vec{u}_i are displacement vectors. K_j is the coupling constant that quantifies the strength of the interaction between the two atoms. The equation of motion for atom i is therefore:

$$m\frac{d^2\vec{u}_i}{dt^2} = \sum_j \vec{F}_j \ , \tag{35}$$

where the summation runs on the nearest and next nearest neighbors⁴ of i and thus becomes:

$$m\frac{d^2\vec{u}_i}{dt^2} = K \sum_{j'} (\vec{u}_{j'} - \vec{u}_i) + K' \sum_{j''} (\vec{u}_{j''} - \vec{u}_i) .$$

⁴According to the numbering in Figures 4a or 9a.

Index j' runs on first neighbors, while j'' on second neighbors.

At this point it is assumed \vec{R}_i as the origin and that the displacement vector of the j-th atom at position \vec{R}_j is of the form

$$\vec{u}_i = \vec{A}e^{i\left(\vec{R}_j \cdot \vec{q} - \omega t\right)} ,$$

with $\vec{R}_j = (x_j, y_j)$, $\vec{A} = (A_x, A_y)$, $\vec{q} = (q_x, q_y)$. By inserting $\vec{u}_i = \vec{A}e^{-i\omega t}$ into Eq.(35):

$$m\frac{d^2\vec{u}_i}{dt^2} = -m\omega^2\vec{A}e^{-i\omega t} = \sum_j \vec{F}_j . \tag{36}$$

We now need to explicitly calculate all the forces acting on atom i. We give the first force acting in the hexagonal scheme, as an example:

$$\vec{F}_{1} = K \left[\hat{R}_{1} \cdot (\vec{u}_{1} - \vec{u}_{i}) \right] \hat{R}_{1} =$$

$$= K \left[\hat{R}_{1} \cdot \left(\vec{A} e^{i \left(\vec{R}_{j} \cdot \vec{q} - \omega t \right)} - \vec{A} e^{-i \omega t} \right) \right] \hat{R}_{1} =$$

$$= K \left[\left(e^{i \vec{R}_{1} \vec{q}} - 1 \right) \left(\hat{R}_{1} \cdot \vec{u}_{i} \right) \right] \hat{R}_{1} =$$

$$= K \left[\left(e^{i a q_{x}} - 1 \right) (1, 0) \begin{pmatrix} A_{x} \\ 0 \end{pmatrix} \right] e^{-i \omega t} ,$$

where $\vec{R}_1 = a(1,0)$ and $\hat{R}_1 = (1,0)$.

Once all the forces have been calculated, we substitute them within Eq.(36) and thus we obtain the dynamic vector equation:

$$\omega^2 A_{\xi} = \sum_{\chi} D_{\xi\chi} A_{\chi} , \qquad \xi, \chi = (x, y) .$$
 (37)

From this the four components of the dynamic matrix are derived:

$$\begin{pmatrix} D_{xx} & D_{xy} \\ D_{yx} & D_{yy} \end{pmatrix} . \tag{38}$$

We calculate phonon dispersion frequencies from the eigenvalues of that matrix:

$$\omega_{+/-}^2 = \frac{D_{xx} + D_{yy}}{2} \pm \sqrt{\left(\frac{D_{xx} - D_{yy}}{2}\right)^2 + D_{xy}D_{yx}} . \tag{39}$$

B Taylor Expansions

The generic Taylor expansion for the potential in Eq.(1) is as follows:

$$V_{\text{tot}} = V_0 + \sum_{i\xi} \Pi_{\xi_i} u_{\xi_i} + \frac{1}{2!} \sum_{ij,\xi\chi} D_{\xi_i,\chi_j} u_{\xi_i} u_{\chi_j} + \frac{1}{3!} \sum_{ijk,\xi\chi\zeta} \Psi_{\xi_i,\chi_j,\zeta_k} u_{\xi_i} u_{\chi_j} u_{\zeta_k} + o(u^4) , \quad (40)$$

where i = 1, ..., N runs on the lattice nuclei, j and k run on the nearest and next nearest neighbors of the i-th nucleus. Greek letters are indices running on the three spatial

coordinates: $\xi, \chi, \zeta = x, y, z$, while u_{ξ_i} represents the displacement from equilibrium of the *i*-th nucleus in the ξ direction. The constant term is set to zero; the first-order term is also zero when evaluating the derivatives at equilibrium. We define:

$$V_2 \equiv \frac{1}{2!} \sum_{ij,\xi\chi} D_{\xi_i,\chi_j} u_{\xi_i} u_{\chi_j} , \qquad V_3 \equiv \frac{1}{3!} \sum_{ijk,\xi\chi\zeta} \Psi_{\xi_i,\chi_j,\zeta_k} u_{\xi_i} u_{\chi_j} u_{\zeta_k} ,$$

where D_{ξ_i,χ_j} has already been defined in Eq.(6) and

$$\Pi_{\xi_i} \equiv \left. \left(\frac{\partial V_{\text{tot}}}{\partial u_{\xi_i}} \right) \right|_{\text{eq}} , \qquad \Psi_{\xi_i, \chi_j, \zeta_k} \equiv \left. \left(\frac{\partial^3 V_{\text{tot}}}{\partial u_{\xi_i} \partial u_{\chi_j} \partial u_{\zeta_k}} \right) \right|_{\text{eq}} . \tag{41}$$

We rewrite the total potential in Eq.(1) as

$$V_{\text{tot}} = \frac{1}{2} \sum_{i=1}^{N} V_{ij} , \qquad V_{ij} \equiv \sum_{j} \frac{K_{ij}}{2} \left(r_{ij} - r_{ij}^{\text{eq}} \right)^{2} .$$
 (42)

As we are going to calculate the derivatives of the interaction potential between a pair of atoms V_{ij} , it is useful to simplify the formalism of each individual term of the derivation in the following way,

$$V_{\xi_{i}\chi_{j}} \equiv \left. \frac{\partial^{2}V_{ij}}{\partial \xi_{i}\partial \chi_{j}} \right|_{eq} u_{\xi_{i}}u_{\chi_{j}} , \qquad V_{\xi_{i}\chi_{j}\zeta_{k}} \equiv \left. \frac{\partial^{3}V_{ij}}{\partial \xi_{i}\partial \chi_{j}\partial \zeta_{k}} \right|_{eq} u_{\xi_{i}}u_{\chi_{j}}u_{\zeta_{k}} ,$$

in order to compactly highlight all the development terms that need to be calculated individually for the two-dimensional case.

The second-order term is:

$$V_2 = \frac{1}{2} \sum_{i=1}^{N} \left[V_{x_i^2} + V_{y_i^2} + 2V_{x_i y_i} + \sum_{j \neq i} \left(V_{x_j x_i} + V_{y_j y_i} + V_{y_j x_i} + V_{x_j y_i} \right) \right] . \tag{43}$$

Instead, the third-order term is:

$$V_{3} = \frac{1}{6} \sum_{i=1}^{N} \left\{ V_{x_{i}^{3}} + V_{y_{i}^{3}} + 3V_{y_{i}x_{i}^{2}} + 3V_{y_{i}^{2}x_{i}} + \sum_{j \neq i} \left[2 \left(V_{x_{j}x_{i}^{2}} + V_{y_{j}y_{i}^{2}} + V_{y_{j}x_{i}^{2}} + V_{x_{j}y_{i}^{2}} + 2V_{y_{j}x_{i}y_{i}} + 2V_{x_{j}x_{i}y_{i}} \right) + + V_{x_{j}^{2}x_{i}} + V_{y_{j}^{2}y_{i}} + V_{y_{j}^{2}x_{i}} + V_{x_{j}^{2}y_{i}} + 2V_{x_{j}y_{j}x_{i}} + 2V_{x_{j}y_{j}y_{i}} \right] \right\}.$$

$$(44)$$

For any kind of pair-interaction potential (Eq.(1) is just an example, Lennard-Jones interaction is another) there are no coupling terms involving three or more distinct atoms simultaneously and so V_{tot} has nonzero terms containing only two distinct or equal particles, labelled by indices i and j.

Now it is convenient to calculate separately all derivatives of V_{ij} , considering $\xi \in (x, y)$:

• First order:

$$\frac{\partial V_{ij}}{\partial \xi_i} = \sum_{\langle i,j \rangle} K_{ij} \frac{\left(r_{ij} - r_{ij}^{eq}\right) \left(\xi_i - \xi_j\right)}{r_{ij}} \ .$$

· Second order:

$$\frac{\partial^{2}V_{ij}}{\partial\xi_{i}^{2}} = \sum_{\langle i,j \rangle} K_{ij} \left\{ \left(\frac{\xi_{i} - \xi_{j}}{r_{ij}} \right)^{2} + \frac{r_{ij} - r_{ij}^{eq}}{r_{ij}} \left[1 - \left(\frac{\xi_{i} - \xi_{j}}{r_{ij}} \right)^{2} \right] \right\};$$

$$\frac{\partial^{2}V_{ij}}{\partial\xi_{j}\partial\xi_{i}} = \sum_{\langle i,j \rangle} K_{ij} \left\{ - \left(\frac{\xi_{i} - \xi_{j}}{r_{ij}} \right)^{2} + \frac{r_{ij} - r_{ij}^{eq}}{r_{ij}} \left[\left(\frac{\xi_{i} - \xi_{j}}{r_{ij}} \right)^{2} - 1 \right] \right\};$$

$$\frac{\partial^{2}V_{ij}}{\partial x_{i}\partial y_{i}} = \frac{\partial^{2}V_{ij}}{\partial y_{i}\partial x_{i}} = -\frac{\partial^{2}V_{ij}}{\partial x_{j}\partial y_{i}} = -\frac{\partial^{2}V_{ij}}{\partial y_{j}\partial x_{i}} =$$

$$= \sum_{\langle i,j \rangle} K_{ij} \left\{ \frac{(x_{i} - x_{j})(y_{i} - y_{j})}{r_{ij}^{2}} \left[1 - \frac{r_{ij} - r_{ij}^{eq}}{r_{ij}} \right] \right\}.$$

• Third order:

$$\frac{\partial^{3}V_{ij}}{\partial \xi_{i}^{3}} = \frac{\partial^{3}V_{ij}}{\partial \xi_{j}^{2}\xi_{i}} = -\frac{\partial^{3}V_{ij}}{\partial \xi_{j}\partial \xi_{i}^{2}} =$$

$$= \sum_{\langle i,j \rangle} 3K_{ij} \left(\frac{\xi_{i} - \xi_{j}}{r_{ij}^{2}} \right) \left\{ 1 - \left(\frac{\xi_{i} - \xi_{j}}{r_{ij}} \right)^{2} + \frac{r_{ij} - r_{ij}^{eq}}{r_{ij}} \left[\left(\frac{\xi_{i} - \xi_{j}}{r_{ij}} \right)^{2} - 1 \right] \right\} ;$$

$$\frac{\partial^{3}V_{ij}}{\partial x_{i}^{2}\partial y_{i}} = \frac{\partial^{3}V_{ij}}{\partial y_{j}\partial x_{j}\partial x_{i}} = \frac{\partial^{3}V_{ij}}{\partial x_{j}^{2}\partial y_{i}} = -\frac{\partial^{3}V_{ij}}{\partial y_{j}\partial x_{i}^{2}} = -\frac{\partial^{3}V_{ij}}{\partial x_{j}\partial x_{i}\partial y_{i}} =$$

$$= \sum_{\langle i,j \rangle} K_{ij} \left(\frac{y_{i} - y_{j}}{r_{ij}^{2}} \right) \left\{ 1 - 3 \left(\frac{x_{i} - x_{j}}{r_{ij}} \right)^{2} + \frac{r_{ij} - r_{ij}^{eq}}{r_{ij}} \left[3 \left(\frac{x_{i} - x_{j}}{r_{ij}} \right)^{2} - 1 \right] \right\} ;$$

$$\frac{\partial^{3}V_{ij}}{\partial x_{i}\partial y_{i}^{2}} = \frac{\partial^{3}V_{ij}}{\partial x_{j}\partial y_{j}\partial y_{i}} = \frac{\partial^{3}V_{ij}}{\partial y_{j}^{2}\partial x_{i}} = -\frac{\partial^{3}V_{ij}}{\partial x_{j}\partial y_{i}^{2}} = -\frac{\partial^{3}V_{ij}}{\partial y_{j}\partial y_{i}\partial x_{i}} =$$

$$= \sum_{\langle i,j \rangle} K_{ij} \left(\frac{x_{i} - x_{j}}{r_{ij}^{2}} \right) \left\{ 1 - 3 \left(\frac{y_{i} - y_{j}}{r_{ij}} \right)^{2} + \frac{r_{ij} - r_{ij}^{eq}}{r_{ij}} \left[3 \left(\frac{y_{i} - y_{j}}{r_{ij}} \right)^{2} - 1 \right] \right\} .$$

Evaluating Eq.(43) and Eq.(44) at equilibrium and taking into account the specific geometry of the lattice, the formulas given in Sections 2 and 3 are derived.

C Error Estimation

The MD code integrates the equations of motion of each atom by applying the RKF method, which proceeds in M integration steps. At each step it computes some quantities, such as V_{tot} , V_2 and V_3 . Let us generically call p one of these data. Clearly a few p_i are closely correlated within a certain correlation time. Therefore, if we want to estimate an

average of p_i values by applying, for example, Eq.(27), we cannot computed the standard deviation using the usual formula, because p_i values are not independent data.

What we can do is to divide M into $N_{\rm Blk}=30$ blocks. So each block contains $L=\lfloor\frac{M}{N_{\rm Blk}}\rfloor$ integration steps of the RKF algorithm.

At this point within each block we calculate the average:

$$\langle p \rangle_j = \frac{1}{L} \sum_{k=j \cdot L}^{(j+1) \cdot L} p_k , \qquad (45)$$

where index $j = 0, ..., N_{Blk} - 1$ identifies the j-th block. We must pay attention to the fact that the last block may not contain exactly L elements. For the final block the summation in Eq.(45) runs from $N_{Blk} - 1$ to M.

At this point we are able to calculate the average of the averages in each block:

$$\langle p \rangle = \frac{1}{N_{\text{Blk}}} \sum_{j=1}^{N_{\text{Blk}}} \langle p \rangle_j \qquad \langle p^2 \rangle = \frac{1}{N_{\text{Blk}}} \sum_{j=1}^{N_{\text{Blk}}} \langle p \rangle_j^2 .$$
 (46)

Assuming that each block is long enough with respect to the correlation time, the averages in Eq.(45) are independent data and we can finally use them to estimate a standard deviation:

$$StdDev_p = \sqrt{\frac{\langle p^2 \rangle - \langle p \rangle^2}{N_{Blk} - 1}} . \tag{47}$$

In practice, we use this statistics for quadratic quantities, such as in Eq.(27). In other terms, $p(t) = v^2(t)$. Applying standard error propagation, the quadratic average and the standard deviation are:

$$\langle v \rangle = \sqrt{\langle p \rangle} , \qquad \text{StdDev}_v = \frac{1}{2\sqrt{\langle p \rangle}} \sqrt{\frac{\langle p^2 \rangle - \langle p \rangle^2}{N_{\text{Blk}} - 1}} .$$
 (48)

In Section 5, we use these equations to evaluate $\sigma_{\Delta V_2}$ and $\sigma_{\Delta V_3}$, and to estimate the corresponding error bars.

References

- [1] J. Norell, A. Fasolino and A.S. de Wijn, *Phys. Rev. E* 94, 023001 (2016).
- [2] J. Miglio, *Anarmonicità geometrica*, diploma thesis (University Milan, 2022), http://materia.fisica.unimi.it/manini/theses/miglio.pdf.
- [3] N. Manini, Introduction to the physics of matter: basic atomic, molecular, and solid-state physics (Springer, 2020).
- [4] G. Grosso and G.P. Parravicini, Solid State Physics (Academic Press, Oxford, 2014).
- [5] N.W. Ashcroft and M.D. Mermin, *Solid State Physics* (Holt-Saunders, Philadelphia, 1976).
- [6] C. Maderna, Analisi matematica 2 (Città studi, Torino, 2010).
- [7] G.P. Srivastava, *The physics of phonons* (A. Hilger, Bristol Philadelphia New York, 1990).